JGR Biogeosciences

RESEARCH ARTICLE
10.1029/2022JG007326

# Nitrous Oxide Dynamics in the Siberian Arctic Ocean and Vulnerability to Climate Change

**Birgit Wild[1,2], Nicholas E. Ray[1,3], Céline Lett[1], Amelia Jane Davies[1,4], Elena Kirillova[1,5], Henry Holmstrand[1], Elizaveta Klevantceva[6,7], Alexander Osadchiev[8], Ivan Gangnus[9,10], Evgeniy Yakushev[8,9,11], Denis Kosmach[7,9], Oleg Dudarev[7,9], Örjan Gustafsson[1,2], Igor Semiletov[7,9], and Volker Brüchert[2,12]**

[1]Department of Environmental Science, Stockholm University, Stockholm, Sweden, [2]Bolin Centre for Climate Research, Stockholm University, Stockholm, Sweden, [3]Department of Ecology and Evolutionary Biology, Cornell University, Ithaca, NY, USA, [4]Department of Geosciences, Goethe-Universität, Frankfurt am Main, Germany, [5]Ulyanovsk State University, Ulyanovsk, Russia, [6]Tomsk Polytechnic University (TPU), Tomsk, Russia, [7]Il'ichov Pacific Oceanological Institute (POI), Far-East Branch of the Russian Academy of Sciences, Vladivostok, Russia, [8]Shirshov Institute of Oceanology, Russian Academy of Sciences, Moscow, Russia, [9]Tomsk State University (TSU), Tomsk, Russia, [10]Faculty of Geography, Lomonosov State University, Moscow, Russia, [11]Norwegian Institute for Water Research, Oslo, Norway, [12]Department of Geological Sciences, Stockholm University, Stockholm, Sweden

**Abstract** Nitrous oxide ($N_2O$) is a strong greenhouse gas and stratospheric ozone-depleting substance. Around 20% of global emissions stem from the ocean, but current estimates and future projections are uncertain due to poor spatial coverage over large areas and limited understanding of drivers of $N_2O$ dynamics. Here, we focus on the extensive and particularly data-lean Arctic Ocean shelves north of Siberia that experience rapid warming and increasing input of land-derived nitrogen with permafrost thaw. We combine water column $N_2O$ measurements from two expeditions with on-board incubation of intact sediment cores to assess $N_2O$ dynamics and the impact of land-derived nitrogen. Elevated nitrogen concentrations in water column and sediments were observed near large river mouths. Concentrations of $N_2O$ were only weakly correlated with dissolved nitrogen and turbidity, reflecting particulate matter from rivers and coastal erosion, and correlations varied between river plumes. Surface water $N_2O$ concentrations were on average close to equilibrium with the atmosphere, but varied widely ($N_2O$ saturation 38%–180%), indicating strong local $N_2O$ sources and sinks. Water column $N_2O$ profiles and low sediment-water $N_2O$ fluxes do not support strong sedimentary sources or sinks. We suggest that $N_2O$ dynamics in the region are influenced by water column $N_2O$ consumption under aerobic conditions or in anoxic microsites of particles, and possibly also by water column $N_2O$ production. Changes in biogeochemical and physical conditions will likely alter $N_2O$ dynamics in the Siberian Arctic Ocean over the coming decades, in addition to reduced $N_2O$ solubility in a warmer ocean.

**Plain Language Summary** Nitrous oxide ($N_2O$) is a strong greenhouse gas and can reduce the stratospheric ozone layer. Around 20% of global $N_2O$ emissions come from the ocean. These estimates are uncertain due to scarce data from large areas and a limited understanding of controls on $N_2O$ production and consumption. Here, we focus on the shallow but large continental shelves of the Arctic Ocean north of Siberia. This area is rapidly warming, and receives land-derived nitrogen from rivers and coastal erosion that is expected to increase with permafrost thaw. We analyzed $N_2O$ concentrations in the water column during two expeditions, and performed incubations with intact sediment cores to measure $N_2O$ release from sediment to water. Our data show that concentrations of dissolved nitrogen in the water and of total nitrogen in sediments increase toward large river mouths. Concentrations of $N_2O$ were weakly correlated with a range of parameters including dissolved inorganic nitrogen and turbidity, with high variability among river plumes. On average, water-air $N_2O$ fluxes were low, but strong $N_2O$ sources and sinks were observed locally. An increase in water temperature could substantially reduce $N_2O$ solubility in the ocean water, and add to biogeochemical and physical changes that could alter $N_2O$ production itself.

**Key Points:**

- We studied $N_2O$ dynamics on the vast Siberian Arctic Ocean shelves that experience strong warming and nitrogen input from land permafrost
- $N_2O$ was variably influenced by dissolved nitrogen and turbidity from land, and likely consumed in the water column
- Surface water $N_2O$ was on average in equilibrium with the atmosphere, but strong local sources and sinks were observed

**Supporting Information:**

Supporting Information may be found in the online version of this article.

**Correspondence to:**

B. Wild,
birgit.wild@aces.su.se

**Citation:**

Wild, B., Ray, N. E., Lett, C., Davies, A. J., Kirillova, E., Holmstrand, H., et al. (2023). Nitrous oxide dynamics in the Siberian Arctic Ocean and vulnerability to climate change. *Journal of Geophysical Research: Biogeosciences*, *128*, e2022JG007326. https://doi.org/10.1029/2022JG007326

Received 9 DEC 2022
Accepted 27 APR 2023

**Author Contributions:**

**Conceptualization:** Birgit Wild, Volker Brüchert
**Formal analysis:** Birgit Wild, Alexander Osadchiev, Ivan Gangnus, Evgeniy Yakushev, Volker Brüchert
**Funding acquisition:** Birgit Wild, Örjan Gustafsson, Igor Semiletov
**Investigation:** Birgit Wild, Céline Lett, Amelia Jane Davies, Elena Kirillova, Elizaveta Klevantceva, Alexander Osadchiev, Ivan Gangnus, Evgeniy Yakushev, Denis Kosmach, Volker Brüchert



## 1. Introduction

Nitrous oxide ($N_2O$) is the third largest contributor to radiative forcing and the most important ozone layer-depleting substance of the 21st century (Ravishankara et al., 2009). On average 20% of current $N_2O$

**Methodology:** Birgit Wild, Nicholas E. Ray, Céline Lett, Henry Holmstrand, Evgeniy Yakushev, Denis Kosmach, Oleg Dudarev, Volker Brüchert
**Project Administration:** Birgit Wild, Oleg Dudarev, Örjan Gustafsson, Igor Semiletov, Volker Brüchert
**Resources:** Birgit Wild, Henry Holmstrand, Oleg Dudarev, Örjan Gustafsson, Igor Semiletov, Volker Brüchert
**Software:** Volker Brüchert
**Validation:** Birgit Wild, Nicholas E. Ray, Volker Brüchert
**Visualization:** Birgit Wild
**Writing – original draft:** Birgit Wild
**Writing – review & editing:** Nicholas E. Ray, Alexander Osadchiev, Ivan Gangnus, Evgeniy Yakushev, Örjan Gustafsson, Igor Semiletov, Volker Brüchert

emissions to the atmosphere have been suggested to stem from the World Ocean, but current estimates of marine emissions show large uncertainties, spanning from 2.5–4.3 Tg N $yr^{-1}$ (Tian et al., 2020). Scarcity of observational data from vast areas (Tian et al., 2020; Yang et al., 2020) and limited quantitative understanding of the factors driving marine $N_2O$ production and consumption processes currently prevent more robust estimates of $N_2O$ emissions from ocean sources, and their future development under changing environmental conditions.

This study targets the shallow continental shelves of the Arctic Ocean north of Siberia where nitrogen released from thawing land permafrost might fuel a wide range of nitrogen cycling processes and potentially stimulate $N_2O$ emissions. This Arctic Ocean region receives substantial nitrogen input from several large rivers that drain permafrost terrain, such as the Ob, Yenisey and Lena. These three rivers alone deliver 0.7 Tg N $yr^{-1}$ and account for ca. 40% of the total riverine nitrogen flux to the Arctic Ocean (Holmes et al., 2012; McClelland et al., 2016). In addition, coastal erosion has been estimated to contribute ca. 1.6 Tg N $yr^{-1}$ to the Arctic Ocean, primarily to the Siberian region (Terhaar et al., 2021). Land-derived nitrogen might support a large part of Arctic Ocean primary production, especially north of Siberia, as indicated by combination of remote sensing-derived primary production estimates with nitrogen flux modeling (Terhaar et al., 2021). A box model based on observations from the northern part of the Siberian Arctic Ocean shelves however suggests that nutrients from the Pacific are more important (Sun et al., 2021). Land-derived nitrogen might also provide substrates for a range of nitrogen cycling processes, either directly or after remineralization of marine organic matter. These processes include nitrification (the conversion of ammonium to nitrate) in oxic surface sediments and the water column, and denitrification (the conversion of nitrate to $N_2$) in deeper, anoxic sediment sections. Both processes can release $N_2O$ as a by-product and denitrification can also consume $N_2O$ by reduction to $N_2$ (Barnes & Upstill-Goddard, 2018). On shallow continental shelves, nitrogen dynamics are usually dominated by sediment processes (Rowe et al., 1975). This has also been indicated for the outer part of the East Siberian Arctic Shelf where sediment processes contributed substantially to nitrogen remineralization (Sun et al., 2021).

Arctic warming occurs at rates 2–3 times the global average and is expected to promote permafrost thaw along the coasts and inland, with repercussions for ocean nitrogen cycling. With progressing permafrost thaw, fluvial transport of dissolved organic nitrogen as well as nitrate is expected to increase, at least in areas dominated by mineral soils (Frey & McClelland, 2009). Additionally, an increase in coastal erosion can already be observed as a consequence of warming (Farquharson et al., 2018; Günther et al., 2013; Jones et al., 2009; Novikova et al., 2018). Increased nitrogen delivery by rivers and coastal erosion may intensify the marine nitrogen cycle in the region, and potentially stimulate nitrification, denitrification, and $N_2O$ release.

Estimates of current $N_2O$ emissions from the Siberian part of the Arctic Ocean shelves and their future trajectory are limited by scarcity of observational data. The only published data from this region are from a cross-shelf transect in the East Siberian Sea around 170°E and indicate elevated concentrations of $N_2O$ compared to the equilibrium with the atmosphere (Yang et al., 2020). However, this eastern part of the East Siberian Sea is strongly influenced by inflow of Pacific water masses. The influence of Pacific waters decreases westwards, while that of freshwater discharge from the large Russian rivers increases (Semiletov et al., 2005). Quantitative data on $N_2O$ dynamics on the extensive Siberian Arctic Ocean shelves, and the impact of land-derived nitrogen, are urgently needed to assess potential $N_2O$ emissions from this region and their trajectory in a warming climate.

This study has three main objectives, (a) to provide observational data of $N_2O$ concentrations and fluxes on the particularly data-lean and vulnerable Siberian part of the Arctic Ocean shelves. These data can contribute to global $N_2O$ budget estimates and future parameterization of model projections. We additionally aimed (b) to constrain potential $N_2O$ sources, and (c) to test the effect of terrigenous nitrogen input on ocean $N_2O$ fluxes. We hypothesized that terrigenous nitrogen input increases nitrogen availability in the water column and sediments near river mouths and coastal erosion sites and promotes $N_2O$ production in these areas. We further hypothesized that sediment processes would represent the main $N_2O$ sources and sinks, as is usually the case on shallow continental shelves. Rare access to the remote study area in the Kara, Laptev and East Siberian Seas was provided by the SWERUS-C3 expedition in July–August 2014 and the International Siberian Shelf Study 2020 (ISSS-2020) expedition in September–November 2020. To address the objectives, we here combine observations of $N_2O$ and dissolved nitrogen concentrations in the water column across the study area with on-board incubation of intact sediment cores to quantify sediment-water $N_2O$ fluxes.

## 2. Materials and Methods

### 2.1. Study Area and Field Sampling

Focus areas of this study were the continental shelves of the Kara, Laptev and East Siberian Seas north of Siberia. The Kara Sea has an average depth of 131 m (Jakobsson, 2002), and is strongly influenced by the Ob and Yenisey rivers that deliver freshwater, carbon and nitrogen (ca. 0.47 Tg N $yr^{-1}$ in particulate and dissolved form; Holmes et al., 2012; McClelland et al., 2016). The Laptev and East Siberian Sea shelves form, together with the Russian part of the Chukchi Sea, the East Siberian Arctic Shelf, the largest and shallowest continental shelf of the world ocean. The Laptev Sea has an average depth of only 48 m (Jakobsson, 2002), and receives ca. 0.27 Tg N $yr^{-1}$ from the Lena river (Holmes et al., 2012; McClelland et al., 2016). The East Siberian Sea has an average depth of 58 m (Jakobsson, 2002) and is the recipient of comparatively small rivers such as Indigirka and Kolyma, but is influenced by the inflow of nutrient-rich Pacific waters from the east. The westward limit of strong Pacific nutrient input varies over time (Peralta-Ferriz & Woodgate, 2017), but might average ca. 160°E (Semiletov et al., 2005). High freshwater input typically results in strong stratification of water masses in the outflow regions of the Siberian Arctic Ocean shelves (Osadchiev, Pisareva, et al., 2020; Sanders et al., 2022; Thibodeau et al., 2017), but mixing of water masses can occur due to wind-driven upwelling (Osadchiev, Silvestrova, & Myslenkov, 2020). The Laptev and East Siberian Seas are further characterized by particularly strong coastal erosion that can locally exceed 5 m per year (Lantuit et al., 2012; Semiletov et al., 2005). This is facilitated by the presence of Pleistocene-age Ice Complex deposits along the coasts that are prone to collapse due to their high ice content. The stations included here where $N_2O$ was measured are primarily located in the Kara, Laptev and East Siberian Seas (Jakobsson, 2002), and a few in the Central Arctic Ocean on the Laptev Sea slope. In line with our research question on the influence of river-derived nitrogen, most stations are located along transects from the mouths of Ob, Lena and Indigirka across the shelf seas.

The data presented here were generated during the SWERUS-C3 and the International Siberian Shelf Study 2020 (ISSS-2020) expeditions. The SWERUS-C3 cruise on-board the Swedish *I/B Oden* is described in detail in previous publications (e.g., Humborg et al., 2017); all stations included here are from the first leg of the expedition in July–August 2014 and are numbered consecutively. The ISSS-2020 expedition represented the 82nd cruise of the Russian *R/V Akademik Mstislav Keldysh* and lasted from late September to early November 2020 covering the shelf of the Kara, Laptev and western part of the East Siberian Sea. Station numbering followed the accumulating order of *R/V Keldysh* expeditions, that is, stations of this cruise were identified as AMK82-6931 to AMK82-7012.

### 2.2. Water Sampling

Concentrations of dissolved $N_2O$ were measured at 9 SWERUS and 56 ISSS-2020 CTD profiling stations covering the whole water column (Figure 1). These depth profiles are complemented by 23 locations for near-surface waters collected during ISSS-2020. Vertical thermohaline measurements were performed with a Seabird SBE911plus (ISSS-2020) and an SBE 911 (SWERUS-C3) equipped with two parallel temperature and conductivity sensors. For ISSS-2020, we here included also data from a chlorophyll fluorometer (Seapoint), a colored dissolved organic matter (CDOM) fluorometer (WET Labs) and a turbidity meter (Seapoint). The turbidity, chlorophyll and CDOM as well as all CTD sensors were calibrated before the cruises in a certified laboratory. Since turbidity, chlorophyll and CDOM sensors were not calibrated against each other, the SWERUS data were not included here. Water samples were collected with 20 L (ISSS-2020) and 7 L (SWERUS-C3) Niskin bottles. Subsurface seawater was additionally collected during ISSS-2020 by a ship-board underway pump-through system with an intake located at a depth of 3 m. The water flow within the pump-through system was provided by a 900-W onboard pump (Metabo). The system was equipped with a thermosalinograph (SBE 21 SeaCAT) that continuously recorded salinity and temperature of flowing subsurface seawater; also these sensors were calibrated before the cruise in a certified laboratory.

### 2.3. Analysis of $N_2O$ Concentrations

Dissolved $N_2O$ concentration were determined by headspace equilibration followed by on-onboard analysis of headspace $N_2O$ concentrations by gas chromatography (Elkins, 1980). Water samples for measurement of dissolved gases were taken from Niskin bottles (ISSS-2020 and SWERUS-C3) or seawater intake (ISSS-2020) as described above. During ISSS-2020, 50 ml plastic syringes were connected via three-way valves to the silicone

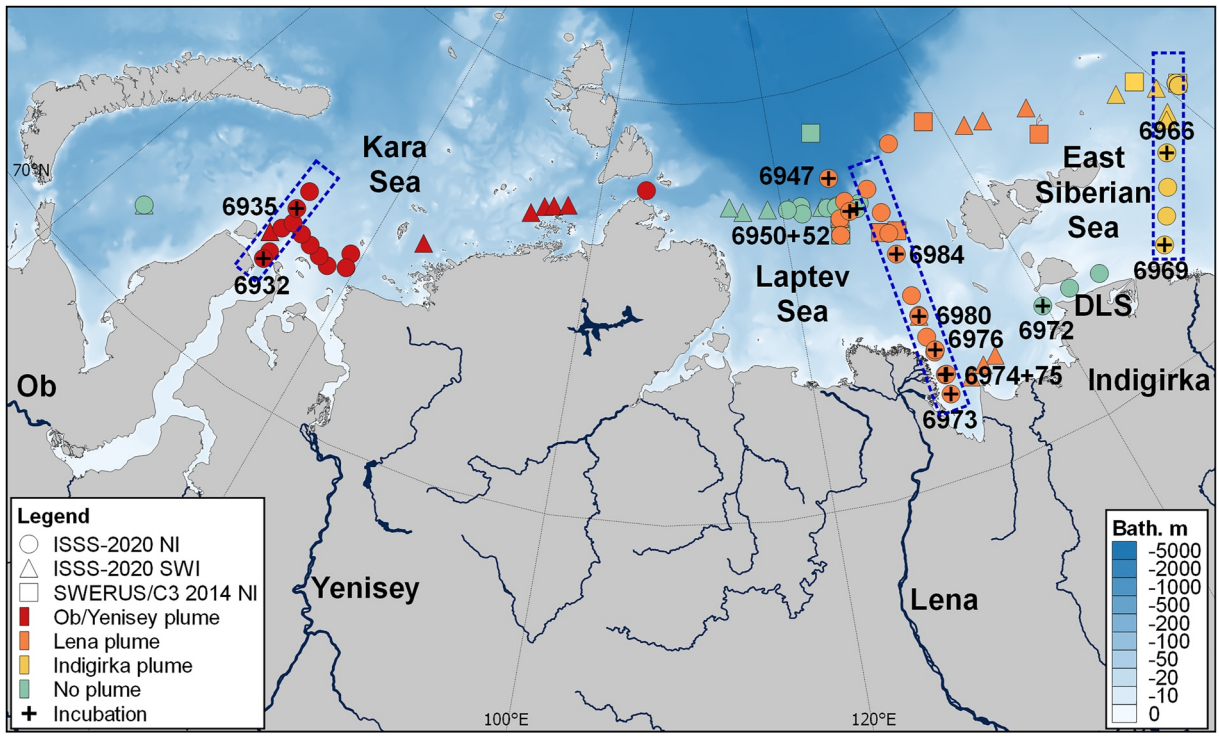


**Figure 1.** Map of the study area. Symbols show stations sampled in 2014 (SWERUS-C3) and 2020 (ISSS-2020), distinguishing between stations sampled using Niskin flasks where depth profiles are available (NI) and stations where only surface water samples were taken (SWI). Stations for sediment incubation are indicated with crosses and labeled with station number (as AMK-82 XXXX). Stations were assigned to river plumes for the purposes of this study based on mixed layer salinity and ocean currents (see Methods for details). The transects shown in Figure 2 are indicated. DLS, Dmitry Laptev Strait. Bathymetry is from IBCAO v4 (Jakobsson et al., 2020).

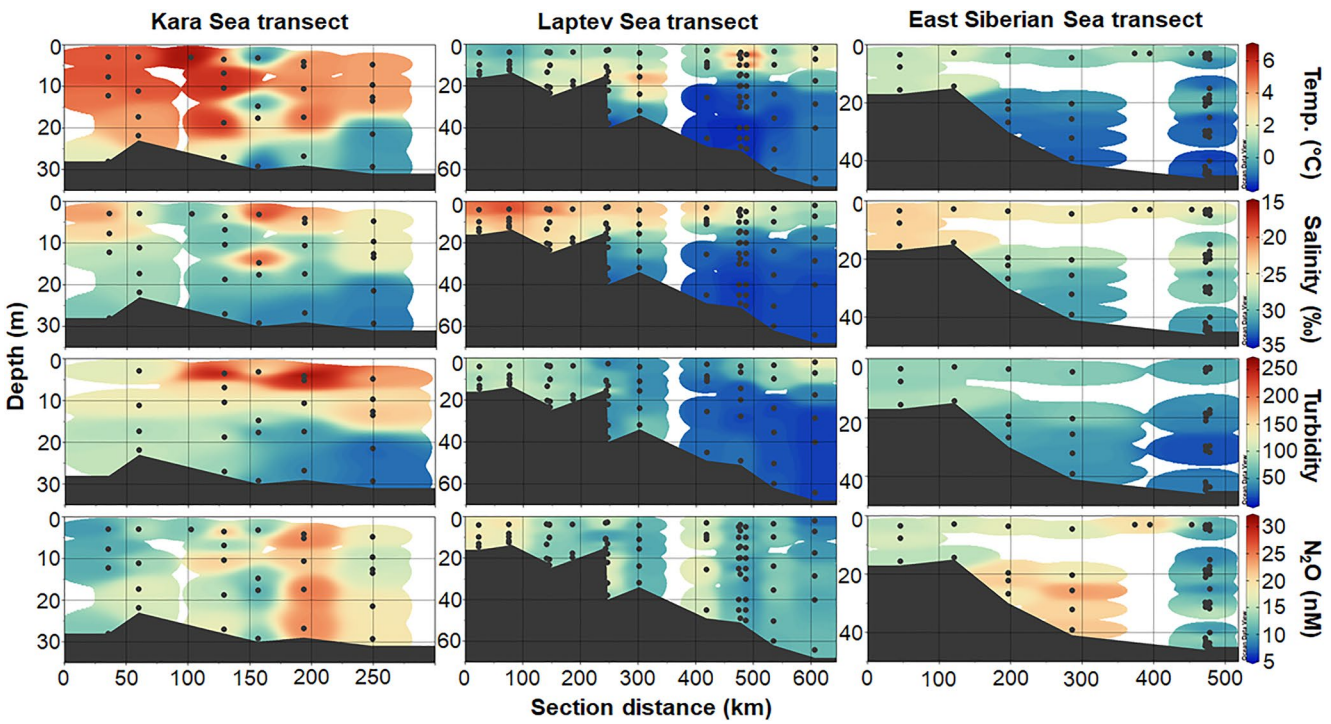


**Figure 2.** Transects of selected parameters in the Kara, Laptev and East Siberian Sea. Shown are temperature, salinity, turbidity, and $N_2O$ concentrations; the location of transects is indicated in Figure 1. The transect figures were generated using Ocean Data View.

tubing on the rosette bottle spigots or the seawater intake, rinsed to remove air bubbles and filled with sample water. Syringes were processed immediately for gas equilibration. The syringe water volume was adjusted to 35 and 15 ml of He were added from a gas bag at atmospheric pressure, and samples were shaken for 30 min at 500 rpm on a shaker table and left to equilibrate for another 30 min at a temperature of 20°C. During SWERUS-C3, water samples were collected bubble-free in 12 ml exetainers with the same technique as above and stabilized with 100 µl 50% $ZnCl_2$ solution before further processing. Before analysis, 4 ml of the sample volume were replaced with He at atmospheric pressure and samples were shaken for 12 hr at 150 rpm on a shaker table to equilibrate headspace and water. In each case, aliquots of the gas phase were then transferred to a SRI Instruments 8610C gas chromatograph equipped with a Porapak Q pre-column, Hayesep D main column and an electron capture detector (ECD). During ISSS-2020, the syringe headspace was transferred to a second syringe and 5 ml were injected through a septum into the sample loop. During SWERUS-C3, the 3 ml of the headspace volume was replaced by salt brine and transferred to a second syringe and loaded via Luerlock on a 1 ml stainless steel injection loop. For detection with ECD, 5% $CH_4$ in Ar was used as make-up gas. Concentrations of $N_2O$ in the gas phase were calculated by calibration against a series of standard gases (Air Liquide). For the ISSS-2020 expedition, standards contained 0.24, 0.60 and 3.01 ppm $N_2O$, with an accuracy of ±10%, ±10%, and ±2%, respectively. For the SWERUS-C3 expedition, standards were 0.30 and 1.04 ppm $N_2O$, each ±3%. Standards were injected for every 20 samples to account for drift. Duplicate standard injections showed a relative standard deviation of 3.2 ± 3.6% (average ± standard deviation) across all sample batches.

Standard curves of the standard gases were calculated before and after each station. On several occasions, more than one station was sampled during a day, and a set of standards was determined after the second station to account for the instrument drift that was estimated from the difference between the estimated concentration and their expected value assuming linear drift over time. If the regression had $p < 0.10$ and $R^2 \geq 0.65$ (Prairie, 1996), we considered drift to be significant, and applied a drift correction using the slope and intercept of this regression. Samples from 19 of 65 stations were thus corrected. 83% of measured concentrations fell within the range of the standards. The remaining 17% were lower than the lowest standard, and the lowest measured value was 0.13 ppm $N_2O$. Dissolved $N_2O$ concentrations were calculated using the Bunsen solubility coefficients of $N_2O$ in seawater at the measured salinity and temperature during equilibration in the laboratory (Weiss & Price, 1980).

Given the differences in sample preparation protocols between ISSS-2020 and SWERUS-C3, we compared both methods with Baltic Sea water samples. Precision was 1.3% for the ISSS-2020 syringe method and 2.5% for the SWERUS-C3 method, calculated as coefficients of variation from five replicates. Concentrations of $N_2O$ measured using the SWERUS-C3 method were 9.0 ± 2.6% lower than using the ISSS-2020 syringe method. We additionally tested the recovery of an $N_2O$ gas standard using the ISSS-2020 method, resulting in 103 ± 2% recovery (average ± standard deviation), suggesting that $N_2O$ concentrations were overestimated by ca. 3% during ISSS-2020 and underestimated by ca. 6% during SWERUS-C3. The differences between both methods do not limit relative comparisons across the study area, as SWERUS-C3 only accounted for 9 of 65 oceanonographic stations. Excluding SWERUS-C3 stations in the statistical analyses gave very similar results. However, even slight over- or underestimations of $N_2O$ concentrations can have implications for $N_2O$ sink versus source strength over large areas. Additional sensitivity analyses on the potential impact of the measurement uncertainties described above on calculated $N_2O$ saturation and sea-to-air fluxes are presented in the Results section.

### 2.4. $N_2O$ Saturation and Sea-Air Fluxes

Surface water $N_2O$ saturation and sea-air $N_2O$ fluxes were calculated by comparison of surface water $N_2O$ concentrations ($[N_2O]_{surf}$) with the concentrations expected for equilibrium with atmospheric $N_2O$ levels ($[N_2O]_{eq}$). Surface waters were defined as the shallowest data available from Niskin casts to a maximum depth of 5 m (final range 2.0–5.0 m), complemented by data from seawater intake (depth 3 m). Atmospheric equilibrium concentrations were calculated as a function of water temperature and salinity as previously described (Weiss & Price, 1980), using an atmospheric mixing ratio of 327.7 ppb $N_2O$ for SWERUS-C3 and 334.1 ppb $N_2O$ for ISSS-2020, that is, the June 2014 and October 2020 averages reported by the NOAA/ESRL halocarbons in situ program at the Barrow Atmospheric Baseline Observatory, Alaska, United States (Dutton et al., 2017).

Sea-air fluxes of $N_2O$ (F) were calculated as described before (Wanninkhof, 2014), as

$$F = k\left([N_2O]_{surf} - [N_2O]_{eq}\right) \quad (1)$$

$$k = 0.251\,(u)^2\,(\mathrm{Sc}/660)^{-0.5} \quad (2)$$

where $k$ is the gas transfer velocity (cm $h^{-1}$), $u$ is wind speed (m $s^{-1}$) at 10 m, and Sc is the Schmidt number calculated as a function of the measured temperature and salinity as described previously (Johnson, 2010).

Previous studies have used ship-based wind speed measurements or interpolated data products to calculate sea-air fluxes, and in the latter case data that were specific to the time point of sampling, longer-term averages or time-weighted approaches that consider the residence time of the target gas in the mixed layer (Manning et al., 2022). Instantaneous wind speeds tend to result in lower fluxes than longer-term averages given that strong winds are disproportionally important for sea-air fluxes (Manning et al., 2022; Wanninkhof et al., 2009). On the other hand, observational coverage of wind data products is poor in the Siberian Arctic Ocean, and previous studies in this region have therefore commonly used ship-based, instantaneous wind measurements to calculate sea-air fluxes of $CH_4$ and $CO_2$ (Humborg et al., 2017; Shakhova et al., 2010; Thornton et al., 2016). Considering also that our $N_2O$ concentration data represent point observations in time and are the first from this region, and that we consequently cannot assess their temporal variability, we followed these earlier studies and used instantaneous, ship-based wind speeds for calculating sea-air fluxes that must be seen as snapshot observations. Wind speed was measured at 10 m height during SWERUS-C3 and at 20 m height during ISSS-2020; the latter values were corrected to 10 m (Saucier, 2003).

In addition to wind, sea ice cover can substantially influence sea-air fluxes. Of the 88 stations where surface water $N_2O$ concentrations were available, only three were affected by sea ice during sampling. Station SWERUS-45 had 20%–40% fractional sea ice cover, and stations SWERUS-50 and SWERUS-53 had >80%. We here restricted our calculations to the ice-free zone, excluding the three ice-covered stations from sea-air flux calculations. Of the remaining 85 stations, 82 had been ice-free for at least two months, and we consequently do not consider sea-ice history in our calculations (Manning et al., 2022; Ouyang et al., 2021).

### 2.5. Nutrient Measurements

For nutrient measurements, samples were collected directly from Niskin flasks and sea water intake, using high density polyethylene bottles that were acid-washed before the expedition and rinsed multiple times between samples. For all SWERUS-C3 stations and the low-turbidity ISSS-2020 stations, filtering was not necessary as samples were fully transparent, meaning no interference with photometric analyses. Water from high-turbidity stations during ISSS-2020 was filtered with 0.7 µm GF/F syringe filters (see Table S1 in Supporting Information S1 for identification of filtered and non-filtered stations). All samples were analyzed for nutrients at sea within a few hours of sampling. Inorganic nitrogen species were measured with a four-channel segmented flow autoanalyzer (QuAAtro from SEAL Analytical), following the manufacturer's protocols. The determination of nitrate was based on reduction to nitrite and subsequent colorimetric analysis. For SWERUS-C3, only the sum of nitrate and nitrite was analyzed. For ISSS-2020, nitrite was also measured separately and nitrate calculated by subtraction. Ammonia concentrations were analyzed using the phenol-hypochlorite method on ISSS-2020 and the sodium salicylate method on SWERUS-C3. Accuracy was monitored by repeated measurement of a certified reference solution over the course of both expeditions (VKI QC RW1, 7.1 µM ammonium and nitrate each, diluted 1:2 for SWERUS-C3), and expressed as the median deviation from the expected value. During SWERUS-C3, accuracy was −0.15 µM for ammonium and −0.11 µM for nitrate, and during ISSS-2020, +0.04 µM and +0.10 µM, respectively. Precision was calculated as the coefficient of variation of the reference solution, and was 3.7% for ammonium and 1.2% for nitrate during SWERUS-C3, as well as 2.3% and 1.7% during ISSS-2020, respectively. The detection limit was calculated from the standard deviation of repeated measurements of the lowest standard across each expedition (1.1 µM ammonium, 3.6 µM nitrate), as the Student's $t$ value for a single-tailed 99th percentile $t$ statistic and a standard deviation with $n - 1$ degrees of freedom. The calculated detection limit was 0.08 µM for ammonium and 0.09 µM for nitrate during SWERUS-C3, as well as 0.04 and 0.11 µM during ISSS-2020, respectively. In total, 10% of nitrate and 12% of ammonium concentrations were below these formal limits. These values are included in this study to avoid a bias for high concentrations, but are identified as below the formal detection limit in Table S1 in Supporting Information S1. For ISSS-2020 samples, total nitrogen was additionally measured using alkaline persulfate digestion followed by colorimetric determination of the resulting nitrate (Valderrama, 1981). We assumed that total nitrogen equaled total dissolved nitrogen (Voss et al., 2013) and calculated dissolved organic nitrogen by subtracting ammonia, nitrite and nitrate.

Dissolved organic nitrogen might be thus slightly overestimated for low-turbidity stations where water samples were not filtered (Table S1 in Supporting Information S1; see above).

### 2.6. Intact Sediment Core Incubation

We performed an on-board incubation experiment with sediments from 16 stations of the ISSS-2020 expedition (Figure 1) to quantify net sediment-water $N_2O$ fluxes. The approach uses intact multicores to minimize disturbance of the sediment-water interface, and is commonly used in other systems to measure sediment-water fluxes (see e.g., Ray et al., 2021 for general considerations). Sediment cores were taken with an Oktopus multicorer with ca. 10 cm diameter. One core per station was further processed for incubation. Immediately after multicore sampling, liners were closed at the bottom with gas-tight lids and additional bottom water was collected from multiple parallel cores in a carboy. Cores were stored outside at temperatures above the freezing point with overlying bottom water before processing within 1 day. Before the start of the incubation, the sediment depth inside the liner was measured, the liners were complemented with collected bottom water to the rim and closed at the top with gas-tight lids, taking care to avoid bubbles in the core. Average water volume was 3.2 ± 0.3 L (±standard deviation). Top lids were equipped with $O_2$ sensor stickers (PreSens SP-PSt3-NAU-D10-YOP), a magnetic stirrer, an outlet and an inlet port that was connected to a carboy with spare bottom water from the same station. Cores were placed in a water-filled incubator tank (average ± standard deviation 3.3 ± 1.5°C) around a rotor (40 rpm) that gently moved the magnetic stirrers inside the liners, maintaining mixing of the water without re-suspension of sediments. A parallel set of liners was filled only with bottom water (4.3 L) and treated in the same way as a water-only control. Tanks were covered with lids to avoid photosynthesis. Incubations lasted 2 weeks for the nine first stations, but had to be shortened to a minimum of 10 days for later stations to allow for sample processing before the end of the expedition. This incubation time is longer than in previous studies at warmer locations, and was adjusted to the cold conditions of the Arctic Ocean that require longer times to arrive at comparable total changes in dissolved gas concentrations. Dissolved $O_2$ concentrations were monitored throughout the incubation with a PreSens OXY-1 SMA trace transmitter to ensure that conditions never became hypoxic (<65 µM), but also that microbial activity was high enough (represented by consumption of at least 65 µM $O_2$) to allow detectable changes in other gases.

Water samples for $N_2O$ analysis were taken at five time points during the incubation by filling 50 ml syringes from the outlet ports and analyzed as described above; inlet ports were opened during sampling to allow replacement of the removed water from the carboy, ensuring there was never an air headspace. We determined the rate of sediment-water $N_2O$ and $O_2$ fluxes using a regression approach. We considered fluxes to be significant when the change in concentration had $p < 0.10$ and $R^2 \geq 0.65$ (Mazur et al., 2021; Prairie, 1996), and then pro-rated the flux to the cross-sectional area (0.0071 $m^2$) and volume of water in the core. This process was repeated for the water-only control cores, and when they had significant fluxes, we subtracted this rate from the accompanying sediment core. Organic carbon and nitrogen content as well as $\delta^{13}C$ values of organic carbon were analyzed in acidified aliquots of dried surface sediment samples (0–1 cm depth), using a Finnigan Delta Plus XP mass spectrometer coupled to a Thermo Fisher Scientific Flash 2000 Isotope Ratio Mass Spectrometer Element Analyzer via a Conflo II interface. We note that acidification can lead to a slight reduction in measured nitrogen concentrations.

### 2.7. Data Processing and Statistical Analyses

To test the effect of terrestrial nitrogen input on nitrogen cycling, we aimed to reduce the influence of other biogeochemical gradients, such as changes along the water column and east-west gradients in nutrient availability. To that end, we separated (a) observations from the mixed water layer above the pycnocline, as well as (b) observations from individual river plumes. For each sampling station, the bottom of the mixed layer was defined as the depth where the density difference to the surface exceeded 20% of the density difference between the deepest sample and the surface (Shaw et al., 2009), using CTD data at 1 m resolution. The river plumes of the Ob/Yenisey, Lena and Indigirka were described by applying a filter of max. 30‰ salinity in the mixed layer. Based on the direction of ocean currents, the Ob/Yenisey plume was restricted to the Kara Sea west of the Yamal peninsula, and the Lena plume to the Laptev Sea east of 125°E, as well as north of the New Siberian Islands. In addition to nitrogen input from the Lena river, this area is also influenced by coastal erosion in the Buor-Khaya Bay. Stations in the Dmitry Laptev Strait (DLS) south of the New Siberian Islands also receive water from the Lena, but were excluded due to extremely high rates of coastal erosion that limit the comparability with other stations of the river

plume. The Indigirka plume is present in the East Siberian Sea east of the New Siberian Islands; in addition to input from the Indigirka, this area is also influenced by coastal erosion in the DLS as well as Pacific waters from the east. For each station located within a plume, we then calculated the distance from the respective river mouth (estimated as: Ob 73.6°E 72.4°N, Lena 128.5°E 72.53°N, Indigirka 150.6°E 71.3°N).

Statistical analyses were performed in R (R Core Team, 2018). Relationships between environmental parameters were investigated using Pearson's correlations, after log- or rank-transformation where necessary to achieve normal distribution. Correlations were considered significant at $p < 0.05$ and marginally significant at $p < 0.1$. All data used here on salinity, temperature, turbidity, CDOM, chlorophyll A, dissolved organic nitrogen, ammonium, nitrate, nitrite and $N_2O$ concentration are presented in Tables S1 and S2 in Supporting Information S1, and on $N_2O$ saturation and fluxes in Table S3 in Supporting Information S1. Data from sediment core incubations are in Tables S4 and S5 in Supporting Information S1. Statistical results on correlations between water sample parameters are in Tables S6–S9 in Supporting Information S1, and on correlations with water depth in Table S10 in Supporting Information S1.

## 3. Results

### 3.1. River Influence on Salinity, Temperature and Turbidity

The Kara, Laptev and East Siberian Seas showed stratification of water masses with strong river influence in the mixed layer. Fully mixed conditions were only observed at stations AMK82-6968 and 6969 that were located in the DLS close to coastal erosion sites, and where water depth was only 15 and 17 m. The mixed layer showed lower salinity than the deeper waters at all stratified stations, whereas temperature gradients with depth varied geographically (Figure 2 and Table S1 in Supporting Information S1).

Individual river plumes differed substantially in spatial patterns of salinity, temperature, and suspended material in the mixed layer at the time of sampling. With increasing proximity to the river mouth, the Indigirka plume showed a significant decrease in salinity, and increase in temperature, turbidity and CDOM in the mixed layer ($R^2$ 0.50–0.72; Figures 3 and 4 and Table S6 in Supporting Information S1). In addition to river input, turbidity in this region is also fueled by strong erosion in the DLS west of the Indigirka (Figure 3b). The Lena river plume showed a similar decrease in mixed layer salinity with proximity to the river mouth ($R^2$ 0.64), but a decrease in water temperature ($R^2$ 0.32; Figure 4). Highest turbidity was observed at greater distance from the shore (Figure 3b). The Ob/Yenisey plume showed no correlation of salinity and temperature with distance from the river mouth (Figure 4), but fresher and colder mixed layer water masses further to the east are in line with the movement of the river plume following ocean currents. The highest turbidity was observed at two stations 150–220 km north of the Ob mouth (Figures 2 and 3b), and was not associated with low salinity or changes in temperature. All river plumes showed close correlations of turbidity and CDOM ($R^2$ 0.83–0.96), and an increase in chlorophyll A fluorescence with proximity to the river ($R^2$ 0.22–0.67, Table S6 in Supporting Information S1).

### 3.2. River Influence on Dissolved Nitrogen Concentrations

Concentrations of organic nitrogen, ammonium, nitrite and nitrate in the mixed water layer significantly increased with decreasing salinity and increasing proximity to the Ob, Lena and Indigirka river mouths (Figures 3 and 5, and Figures S1–S4 in Supporting Information S1). This applied both across the entire dataset ($R^2$ 0.26–0.53) and in most cases also to individual river plumes (Table S7 in Supporting Information S1). Similar correlations were observed when the entire water column was considered (Table S7 in Supporting Information S1), with the exception of nitrate, which strongly increased in higher-salinity bottom waters (Figure S5 in Supporting Information S1). Correlations with salinity likely underestimate the influence of rivers on dissolved nitrogen in the mixed layer as salinity is also affected by sea ice melt. For the DLS that has high coastal erosion and is also influenced by the Lena river, we observed no elevation of nitrate, nitrite and dissolved organic nitrogen in the mixed layer, but high ammonium concentrations compared to stations near the Lena mouth (Figure 3c and Figure S6 in Supporting Information S1).

### 3.3. Nitrous Oxide in the Water Column

Nitrous oxide concentrations ranged between 5 and 32 nM (mean ± standard deviation 14 ± 4 nM) across all measured water samples. We originally hypothesized that $N_2O$ concentrations would be elevated in near-coastal waters affected by terrigenous nitrogen input, and tested for correlation of $N_2O$ concentration with distance from river mouth, salinity and dissolved nitrogen concentration in the mixed layer. We found that $N_2O$ concentrations significantly increased with nitrate and nitrite concentrations, with proximity to the river mouth and with decreasing salinity

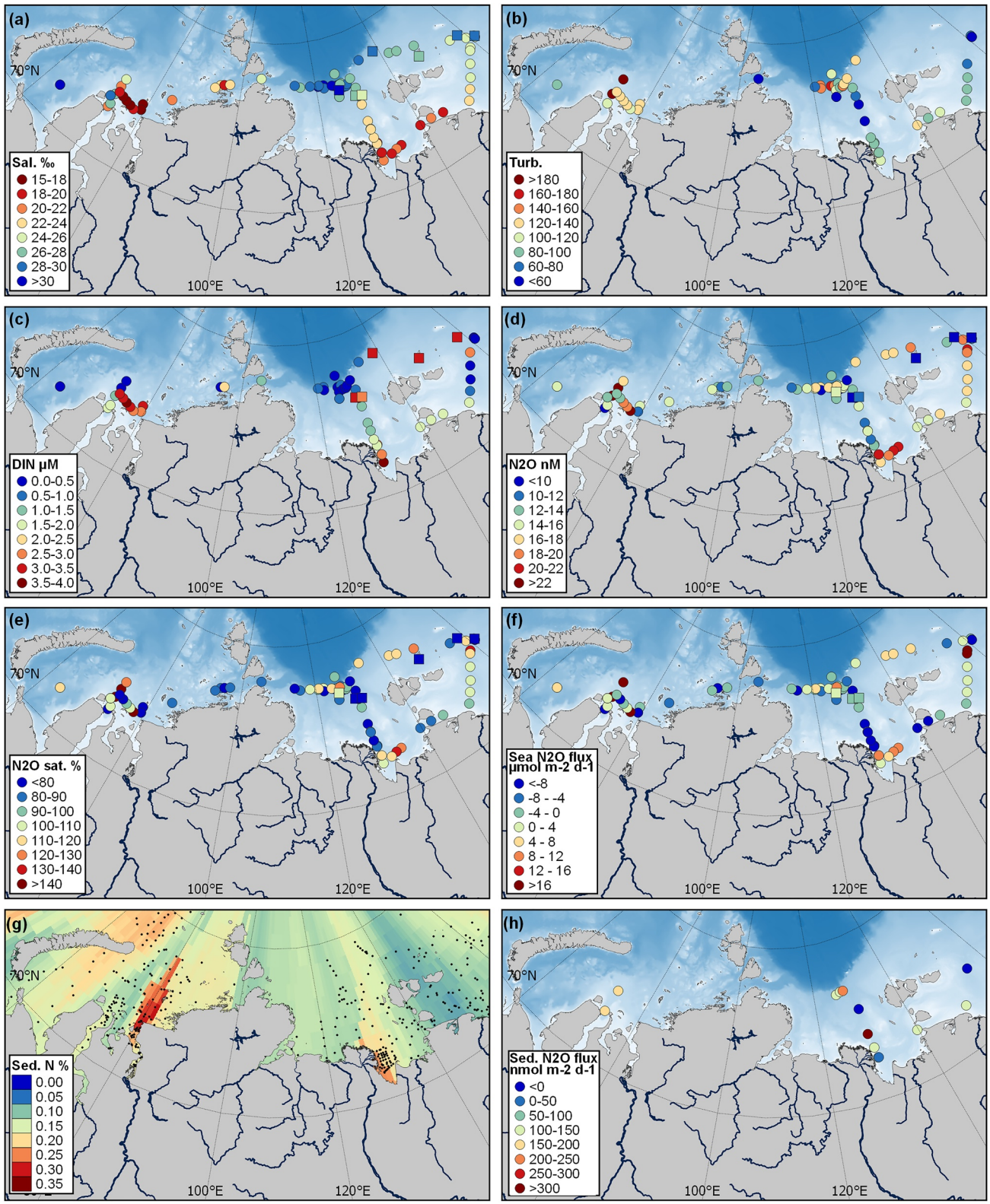


**Figure 3.** Spatial distribution of selected parameters across the study area. Panels show (a) salinity, (b) turbidity, (c) dissolved inorganic nitrogen (DIN) and (d) $N_2O$ concentration in surface waters, (e) surface water $N_2O$ saturation, (f) sea-air $N_2O$ fluxes, (g) interpolated concentrations of sedimentary nitrogen taken from the CASCADE database (Martens et al., 2021a, 2021b) and (h) sediment-water $N_2O$ fluxes determined during incubation of intact sediment cores. Data for 14 of the 16 incubated cores are shown, excluding two that were affected by leakage (see Methods). Circles show data from the ISSS-2020 expedition (September–November 2020) and squares from SWERUS-C3 (July–August 2014). Bathymetry is from IBCAO v4 (Jakobsson et al., 2020).

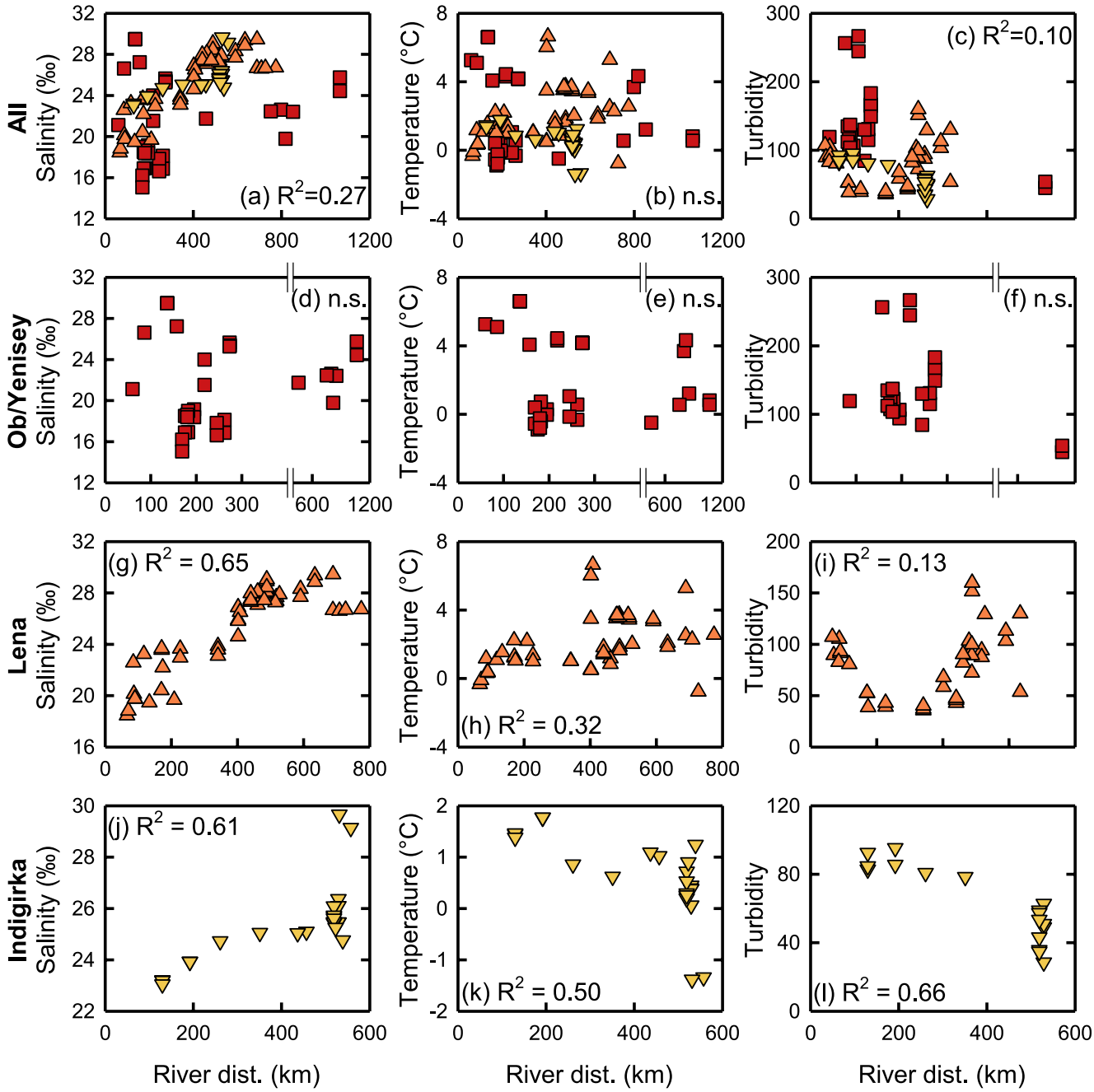


**Figure 4.** Correlations of distance from river mouth, salinity, temperature and turbidity in the mixed layer. Shown are correlations across all samples (a–c) and separately for the Ob/Yenisey (d–f, red squares), Lena (g–i, orange upward triangles) and Indigirka (j–l, yellow downward triangles) plumes. The $R^2$ values are shown for correlations where $p < 0.1$ (n.s., not significant).

across all stations, but the observed correlations were very weak ($p < 0.05$, $R^2 \leq 0.05$; Figure 6 and Figure S7 in Supporting Information S1, and Table S8 in Supporting Information S1). Similar, weak correlations were observed when all depths were considered, as well as a negative correlation with ammonium ($p < 0.05$, $R^2 < 0.1$; Table S8 in Supporting Information S1). The strongest relationships of $N_2O$ were observed in the Indigirka plume, where mixed layer $N_2O$ concentrations showed significant, positive correlations with proximity to the river mouth, water freshness, ammonium, nitrite and nitrate concentration ($p < 0.05$, $R^2$ 0.22–0.44). These correlations were driven by particularly low $N_2O$ concentrations at the most distant stations AMK82-6961 to -6964, SWERUS-50 and -53 (Figures 3d and 6m). These stations are located >500 km from the river mouth and furthest to the north-east (75°N 161°E), and might be influenced by Pacific waters (Semiletov et al., 2005). Nitrous oxide slightly increased with distance from the

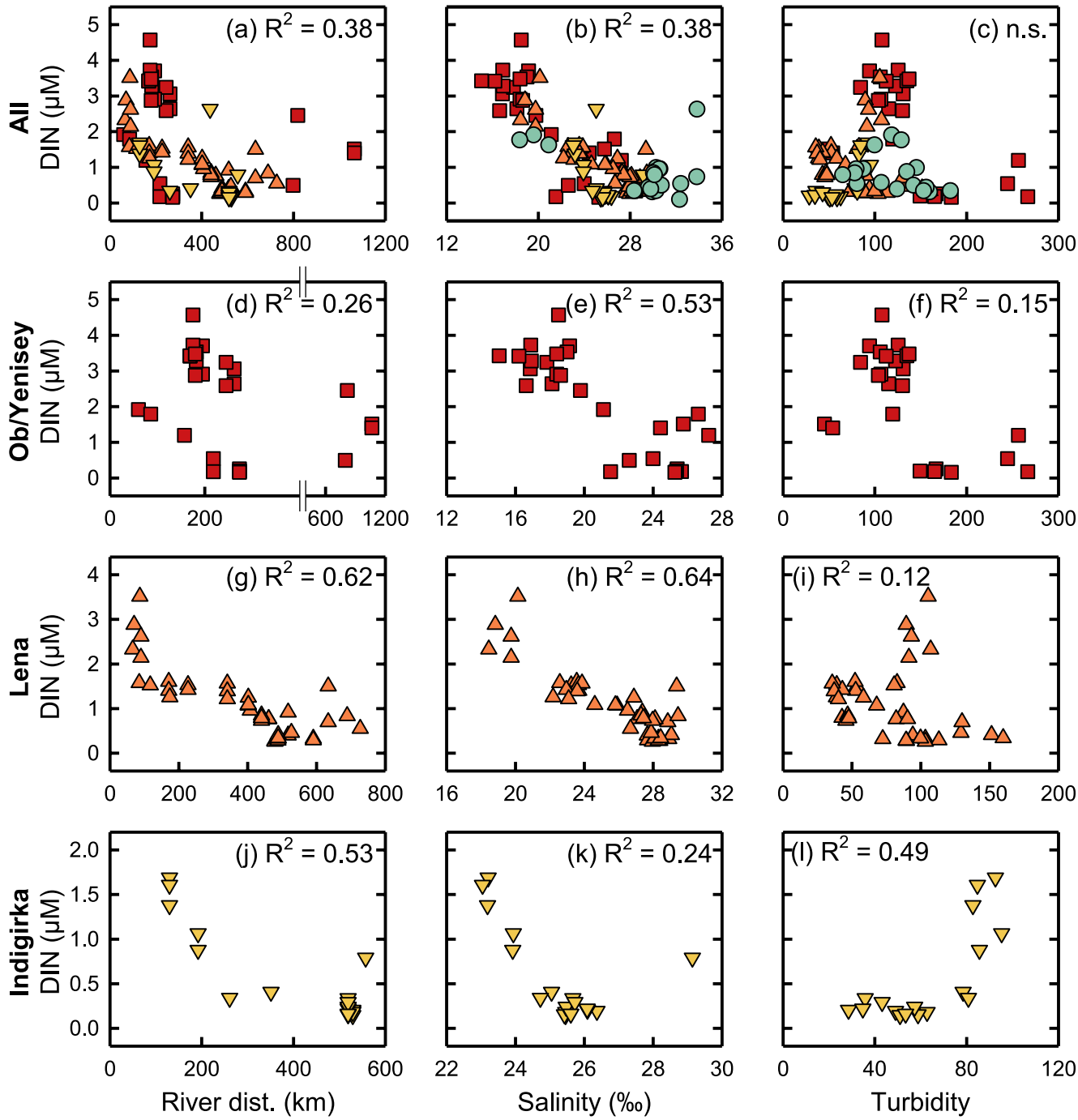


**Figure 5.** Correlations of dissolved inorganic nitrogen (DIN) concentrations with selected parameters in the mixed layer. Shown are correlations across all samples (a–c) and separately for the Ob/Yenisey (d–f, red squares), Lena (g–i, orange upward triangles) and Indigirka (j–l, yellow downward triangles) plumes. Blue circles are stations outside river plumes. The $R^2$ values are shown for correlations where $p < 0.1$ (n.s., not significant).

Indigirka among closer-to-shore locations (Figure 3d). Correlations of $N_2O$ concentrations were weaker for the Lena plume and significant for salinity, nitrite, and nitrate in the mixed layer ($p < 0.05$, $R^2$ 0.11–0.14). No significant positive correlation of $N_2O$ with water freshness or any measured nitrogen form was observed in the Ob/Yenisey plume.

Considering the weak relationship of $N_2O$ with dissolved nitrogen concentrations especially in the Lena and Ob/Yenisey plumes, a wider range of parameters was explored as potential controls on $N_2O$ dynamics. We found that mixed layer $N_2O$ concentrations were significantly correlated with turbidity and CDOM in the Ob/Yenisey and

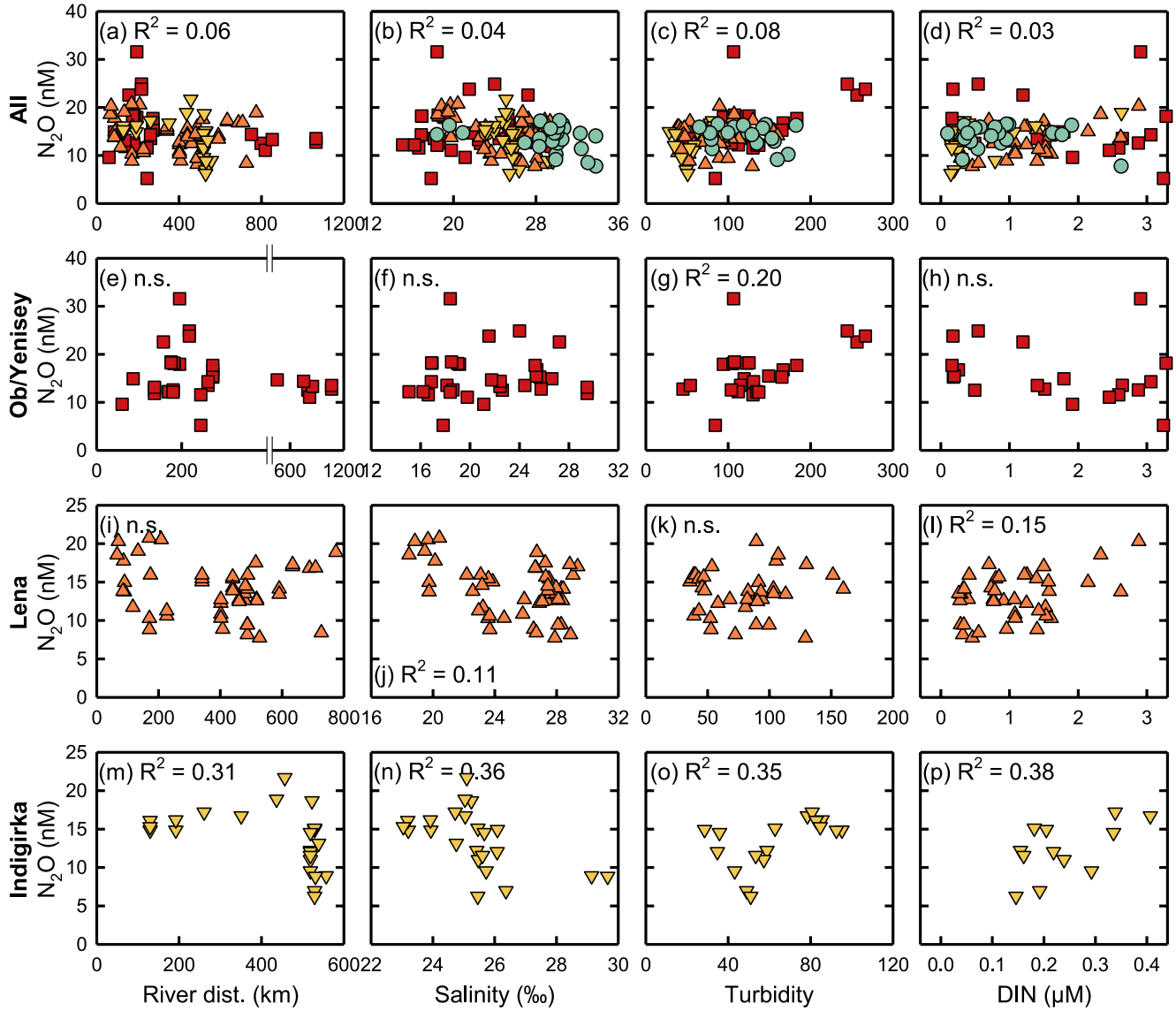


**Figure 6.** Correlations of $N_2O$ concentrations with selected parameters in the mixed layer. Shown are correlations across all samples (a–d) and separately for the Ob/Yenisey (e–h, red squares), Lena (i–l, orange upward triangles) and Indigirka (m–p, yellow downward triangles) plumes. Blue circles are stations outside river plumes. The $R^2$ values are shown for correlations where $p < 0.1$ (n.s., not significant).

Indigirka plumes ($p < 0.05$, $R^2$ 0.20–0.35; Figure 6, Table S8 in Supporting Information S1). No correlation of $N_2O$ concentration and turbidity or CDOM was observed for the Lena.

Finally, depth profiles of $N_2O$ concentrations in the water column were assessed for indications of sedimentary $N_2O$ release or uptake. Depth profiles were available for 65 oceanographic stations (see examples along transects in Figure 2 and all data in Table S1 in Supporting Information S1). Twelve of these stations showed a significant increase in $N_2O$ concentration with depth, and two showed a decrease ($p < 0.1$; Table S10 in Supporting Information S1). Seven stations showed an increase in $N_2O$ saturation with depth, and seven a decrease ($p < 0.1$). The strongest difference between bottom and mixed layer waters was observed at station SWERUS-13, with 32 nM $N_2O$ at the bottom and 9–14 nM $N_2O$ closer to the surface.

### 3.4. Nitrous Oxide Saturation and Sea-Air Fluxes

Surface water $N_2O$ saturation averaged 94 ± 24% with a total range of 38%–180% (Figure 3e). The high variability of surface water $N_2O$ saturation was primarily driven by the wide range in $N_2O$ concentrations ($p < 0.001$, $R^2$

**Table 1**
*Overview of Surface Water $N_2O$ Concentrations, Saturation, Sea-Air Fluxes and Wind Speed at 10 m*

| | $N_2O$ conc. (nM) | | $N_2O$ sat. (%) | | Flux (μmol $m^{-2}$ $d^{-1}$) | | Wind (m $s^{-1}$) | |
|---|---|---|---|---|---|---|---|---|
| Ref. (*n*) | Av ± sd | [Range] | Av ± sd | [Range] | Av ± sd | [Range] | Av ± sd | [Range] |
| Kara Sea | | | | | | | | |
| Here (23) | 15 ± 5 | [10–32] | 99 ± 32 | [65–180] | 1.4 ± 18.6 | [−38.2 to 58.1] | 7.3 ± 3.6 | [1.4–16.6] |
| Laptev Sea | | | | | | | | |
| Here (36) | 14 ± 3 | [8–21] | 91 ± 19 | [51–131] | −2.9 ± 7.8 | [−21.8 to 10.8] | 7.1 ± 3.7 | [0.6–12.6] |
| East Siberian Sea | | | | | | | | |
| Here (18–21) | 14 ± 4 | [6–22] | 89 ± 27 | [38–134] | 1.6 ± 10.6 | [−15.4 to 32.9] | 7.8 ± 3.4 | [2.3–13.2] |
| All from this study | | | | | | | | |
| Here (85–88) | 15 ± 4 | [6–32] | 94 ± 24 | [38–180] | −0.5 ± 12.0 | [−38.2 to 58.1] | 7.2 ± 3.6 | [0.6–16.6] |
| Chukchi Sea | | | | | | | | |
| a | | | | | −0.4 ± 0.7 | | | |
| c (4) | 15 ± 3 | [12–18]* | 114 ± 8 | [107–125] | 9.8 ± 8.6 | [2.3–22.1] | 10.3 ± 4.6 | [3.5–13.4] |
| e (75) | 14 ± 2 | [11–17]* | | | 0.0 ± 1.5 | [−2.9 to 5.7] | | |
| f (21) | 14 ± 1 | [11–16]* | 101 ± 8 | [89–118] | 0.0 ± 1.8 | [−3.0 to 4.2] | | |
| i (12) | 14 ± 2 | [11–16] | 103 ± 8 | [95–118] | | | | |
| Bering Sea | | | | | | | | |
| a | | | | | −0.5 ± 0.5 | | | |
| c (4) | 12 ± 2 | [10–13]* | 106 ± 5 | [102–112] | 2.5 ± 3.3 | [0.2–7.4] | 7.0 ± 1.7 | [5.2–9.2] |
| e (32) | 12 ± 2 | [11–17]* | | | 0.4 ± 1.2 | [−1.9 to 3.4] | | |
| Bering + Chukchi Sea | | | | | | | | |
| b (9) | | | | | 2.3 ± 2.7 | [0.1–8.6] | 6.4 ± 4.5 | [1.5–14.0] |
| g (29) | | | | | 8.2 ± 1.4 | [−1.5 to 22.3] | | |
| h | | | | | 3.7 ± 5.0 | | | |
| Beaufort Sea | | | | | | | | |
| d | 17 ± 1 | | 115 ± 7 | | | | | |
| e (40) | 15 ± 2 | [12–18]* | | | −0.7 ± 1.8 | [−4.8 to 3.9] | | |
| Canadian Arctic Archipelago | | | | | | | | |
| a | | | | | −0.2 ± 1.1 | | | |
| d | 21 ± 3 | | 117 ± 15 | | | | | |
| e (44) | 14 ± 1 | [11–17] | | | −0.3 ± 1.0 | [−3.4 to 2.2] | | |

*Note*. Averages ± standard deviations and total ranges are presented for the Kara, Laptev and East Siberian Sea (this study; individual data in Table S3 in Supporting Information S1), and compared with previous studies on the Arctic Ocean shelves and Bering Strait: *a*, Fenwick et al. (2017); *b*, Heo et al. (2021); *c*, Hirota et al. (2009); *d*, Kitidis et al. (2010); *e*, Manning et al. (2022); *f*, Toyoda et al. (2021); *g*, Wu et al. (2017); *h*, Zhan et al. (2021); *i*, Zhang et al. (2015). In the Kara and East Siberian Sea, average emissions were calculated despite average undersaturation as wind speeds were slightly higher at oversaturated stations. *, Unit is nmol $kg^{-1}$.

0.88). We further observed very weak, but significant correlations indicating an increase in $N_2O$ saturation with proximity to the river mouth, turbidity and temperature, which lowers gas dissolution ($p < 0.05$, $R^2$ 0.07–0.08; Table S9 in Supporting Information S1). We did not observe systematic differences between the Kara, Laptev and East Siberian Seas (Table 1).

Most stations (85 of 88) were completely ice-free during sampling and we considered only these stations for calculation of sea-air $N_2O$ fluxes. On average, the ice-free ISSS-2020 and SWERUS-C3 stations took up 0.5 ± 12 μmol $N_2O$ $m^{-2}$ $d^{-1}$ from the atmosphere. Observations at individual stations ranged from an uptake of 38 μmol to the release of 58 μmol $N_2O$ $m^{-2}$ $d^{-1}$. Wind speed, which strongly determines calculated fluxes, averaged 7.2 ± 3.6 m $s^{-1}$ at these stations. These ship-observed, instantaneous wind speeds are slightly higher than the modeled 2001–2020 annual average of 6.1 m $s^{-1}$ for the same oceanographic stations (Hersbach et al., 2018).

We performed an additional sensitivity test to assess how differences in methodology between the two expeditions could have affected calculated $N_2O$ saturation state and sea-to-air flux. Method cross-comparison and a standard recovery test indicate a possible overestimation of ISSS-2020 $N_2O$ concentrations by 3% and underestimation of SWERUS-C3 concentrations by 6%. This implies a minimum detectable saturation level of 103% for ISSS-2020 to establish a source, and a maximum level of 94% for SWERUS-C3 to establish a sink. Only five of 82 ISSS-2020 surface water observations fell between 100% and 103% saturation, that is, the calculated oversaturation was within the uncertainty range. None of the SWERUS-C3 stations showed saturation between 94% and 100%. Decreasing all ISSS-2020 surface water saturation values by 3% and increasing SWERUS-C3 saturation by 6% would reduce overall $N_2O$ saturation to 91 ± 24% (range 37%–174%), and increase $N_2O$ uptake to 2 ± 12 μmol $N_2O$ $m^{-2}$ $d^{-1}$ (ranging from an uptake of 42 to the release of 54 μmol $N_2O$ $m^{-2}$ $d^{-1}$). These values fall well within the uncertainty range of uncorrected calculations and demonstrate a marginal effect of measurement uncertainties on the main observations of this study.

### 3.5. Sediment Incubation

All incubated cores showed significant, linear changes in concentrations of $N_2O$ (average $R^2$ 0.89, range 0.69–1.00) and $O_2$ (average $R^2$ 0.86, range 0.66–0.97) over time (Table S5 in Supporting Information S1). Data from two cores had to be removed from the dataset as increasing $O_2$ concentrations indicated leakage. Consumption of $O_2$ ranged between 0.3 and 5.0 mmol $m^{-2}$ $d^{-1}$, and final $O_2$ concentrations were 150–378 μM corresponding to 45%–96% of initial values. The decline in $O_2$ concentration during incubation has therefore likely had little effect on measured fluxes as concentrations never became hypoxic (<65 μM).

Incubation of intact sediment cores with overlying water resulted in the average release of 110 ± 166 nmol $N_2O$ $m^{-2}$ $d^{-1}$ from the sediment to the water column. Individual values ranged from an uptake of 266 and 141 nmol $m^{-2}$ $d^{-1}$ observed at two stations to a maximum release of 388 nmol $m^{-2}$ $d^{-1}$ (Figure 3h). Sediment-water $N_2O$ fluxes were positively correlated with CTD-derived bottom water temperature and the ratio of organic carbon over total nitrogen in surface sediments, and negatively correlated with nitrate concentration at the incubation start ($p < 0.1$, $R^2$ 0.21–0.25). Sediment-water $N_2O$ fluxes were not significantly correlated with distance from river mouth, sea-air $N_2O$ fluxes, bottom or surface water $N_2O$ concentration or saturation. In addition, we found that control experiments using only bottom waters without sediment showed significant net $N_2O$ consumption at 10 of 14 stations (Table S4 in Supporting Information S1), with an overall average rate of −434 ± 434 nmol $N_2O$ $m^{-2}$ $d^{-1}$ per meter water column (range −1,242 to +252 nmol $m^{-2}$ $m^{-1}$ $d^{-1}$). This $N_2O$ consumption cannot be explained by anoxic conditions as $O_2$ concentrations at the end of the incubation ranged between 238 and 419 μM in the water-only controls.

## 4. Discussion

### 4.1. $N_2O$ Saturation and Sea-Air Fluxes

Surface waters of the Kara, Laptev and East Siberian Sea were on average in equilibrium with $N_2O$ mixing ratios in the atmosphere, but showed high variability. Nitrous oxide saturation averaged 94 ± 24% with a total range of 38%–180% (Figure 3e). This range greatly exceeded the range of 89%–125% previously reported for other Arctic Ocean shelf seas, including the Chukchi and Beaufort Sea, the Canadian Arctic Archipelago and the Bering Strait (Hirota et al., 2009; Kitidis et al., 2010; Toyoda et al., 2021; Zhang et al., 2015; Table 1). Observations of strong surface water undersaturation as in our study are rare, but not unprecedented. For instance, surface water saturation of ca. 35% has been reported for locations in the Pacific (Cornejo et al., 2015) and of 43% in the Red Sea (Bange et al., 2019). We here observed surface water $N_2O$ saturation below 60% at five stations in the outer part of the East Siberian Sea. Three of these stations (SWERUS-45, -50, and -53) were partly covered with sea ice at the time of sampling; the low $N_2O$ concentrations at these stations might be linked to sea ice melt and dilution of water masses with low-$N_2O$ melt water (Randall et al., 2012). The two remaining stations (AMK82-6958 and -6961) had been ice-free for at least two months before sampling. In both cases, $N_2O$ saturation increased with water column depth, but remained low (42%–70%).

Average sea-air fluxes of $N_2O$ in the Kara, Laptev and East Siberian Seas were comparable in magnitude to previous observations from other Arctic Ocean areas, but showed higher variability (−0.5 ± 12 μmol $N_2O$ $m^{-2}$ $d^{-1}$, range −38 to +58 μmol $N_2O$ $m^{-2}$ $d^{-1}$). For the Chukchi and Beaufort Sea, the Canadian Arctic

Archipelago and the Bering Strait, previous studies have reported fluxes ranging from an uptake of 5 to a release of 22 μmol $m^{-2}$ $d^{-1}$ (Fenwick et al., 2017; Heo et al., 2021; Hirota et al., 2009; Manning et al., 2022; Toyoda et al., 2021; Wu et al., 2017; Zhan et al., 2021; Table 1). For comparison, upwelling and oxygen minimum zones can reach $N_2O$ emission fluxes of several hundred μmol $m^{-2}$ $d^{-1}$ (Arévalo-Martínez et al., 2019; Naqvi et al., 2000; Paulmier et al., 2008). Non-hotspot regions of the Atlantic and Pacific Ocean show fluxes from −2 to +3 μmol $N_2O$ $m^{-2}$ $d^{-1}$ (Breider et al., 2015; Charpentier et al., 2010; Forster et al., 2009; Frame et al., 2014). We note that our fluxes were calculated for stations that were ice-free during sampling (85 of 88), using instantaneous, ship-based windspeeds, and that the previous studies cited here used a variety of approaches to estimate wind speed, including instantaneous values from direct measurements and large-scale data products, and for the latter in some cases applying weighting functions that consider mixed layer residence times. Although the Kara, Laptev and East Siberian Seas were on average in equilibrium with the atmosphere during our expedition, local observations of pronounced $N_2O$ uptake and release might suggest strong, local $N_2O$ sources and sinks in the Siberian shelf seas. We emphasize the need for more observations from this understudied region to assess how representative these observations are, including measurements at higher spatial resolution and from multiple years and seasons.

### 4.2. Sources and Sinks of $N_2O$

In shallow continental shelf systems, $N_2O$ is mainly produced and consumed in sediments (Rowe et al., 1975). In addition, $N_2O$ can be produced and consumed in the water column; it can be delivered by rivers, and it can be transported over long distances with ocean currents. In our study, temperature/salinity plots showed no pattern of higher or lower $N_2O$ concentrations in specific water masses (Figure S8 in Supporting Information S1), and consequently do not point at a strong effect of long-distance transport of water masses on the variability of $N_2O$ concentrations in the study area.

Low sediment-water $N_2O$ fluxes observed in incubations with intact sediment cores, and the absence of a correlation with water column $N_2O$ concentrations do not support a dominant sedimentary $N_2O$ source or sink. Nitrous oxide release from sediments to the water column averaged 110 ± 166 nmol $m^{-2}$ $d^{-1}$. These sediment-water fluxes were lower than the calculated sea-air fluxes at the same stations (−14 to +26 μmol $m^{-2}$ $d^{-1}$), and were not correlated with sea-air fluxes, bottom or surface water $N_2O$ concentration or saturation. Correlations ($p < 0.1$) of sediment-water $N_2O$ fluxes with environmental parameters hint at a shift between dominant nitrogen reduction pathways as a possible driver of spatial variability across the study area. Sediment-water $N_2O$ fluxes increased with bottom water temperature and organic carbon/total nitrogen ratio in surface sediments, as well as decreasing nitrate concentration at the incubation start. High temperature and availability of labile organic carbon have been shown to favor heterotrophic denitrification over autotrophic anammox (Babbin et al., 2014; Canion et al., 2014; Rysgaard et al., 2004; Tan et al., 2020). Similarly, high and stable nitrate loading might favor anammox over denitrification (Brin et al., 2014; Rysgaard et al., 2004). Alternatively, high carbon availability might indicate high decomposition and $O_2$ consumption that could reduce $O_2$ penetration depth, and change $N_2O$ fluxes by altering the balance between various $N_2O$-producing and -consuming processes. However, we found no significant correlation between sediment-water $N_2O$ and $O_2$ fluxes. The relationship with organic carbon/total nitrogen ratios could also reflect differences in organic matter quality impacting carbon and nitrogen availability for microorganisms.

Sediment-water $N_2O$ exchange on the Siberian Arctic Ocean shelves was also low compared to previous observations, including lower rates of both release and uptake. Rates observed here were slightly lower than those reported for the continental margin of the Northeast Subarctic Pacific Ocean (524 ± 122 nmol $m^{-2}$ $d^{-1}$; Jameson et al., 2021), as well as those of temperate and subtropical continental shelf seas and estuaries. A previous study estimated the annually-averaged release of 20–570 nmol $N_2O$ $m^{-2}$ $d^{-1}$ from sediments to the water column in the temperate shelf system of the Gulf of Maine, with a range of observations from −300 to 1,100 nmol $m^{-2}$ $d^{-1}$ (Hopkinson et al., 2001). Observations from estuarine environments range from average releases of ca. 10 μmol $N_2O$ $m^{-2}$ $d^{-1}$ (Seitzinger et al., 1984; Sturm et al., 2016) to the uptake of 552 ± 125 nmol $N_2O$ $m^{-2}$ $d^{-1}$ (Foster & Fulweiler, 2016), but include also more moderate rates, for example, 206 ± 77 nmol $N_2O$ $m^{-2}$ $d^{-1}$ (Mazur et al., 2021) and −460 to +1,940 nmol $N_2O$ $m^{-2}$ $d^{-1}$ (Hopkinson et al., 1999) in two temperate estuaries. The lower rates of both $N_2O$ release and uptake in our study might reflect lower denitrification which can produce and consume $N_2O$, and might be outcompeted by anammox at low temperatures. This is in line with

a previously reported increase in sedimentary $N_2O$ uptake fluxes with temperature in a temperate estuary (Foster & Fulweiler, 2016). The lower rates observed here might also be related to lower nitrogen loading, as previous studies on sediment-water $N_2O$ fluxes have often focused on systems with high anthropogenic nitrogen input.

Largely constant $N_2O$ concentrations across the water column fall in line with low sedimentary $N_2O$ production and consumption. The majority of stations (51 of 65) showed no significant change in $N_2O$ concentration with depth; 12 showed an increase and two a decrease ($p < 0.1$). These observations suggest that sediments can be locally important, but overall do not represent a dominant $N_2O$ source on the Kara, Laptev and East Siberian shelf seas. These findings contrast with previous studies from the Bering Strait and Chukchi Sea shelves. In these regions, sediments were indicated as the main $N_2O$ source by an increase in $N_2O$ concentration with depth (Fenwick et al., 2017; Hirota et al., 2009; Wu et al., 2017; Zhang et al., 2015), although annual variability has been observed with a weak halocline promoting vertical mixing and more homogenous concentrations during one expedition (Toyoda et al., 2021). It seems likely that $N_2O$ dynamics in this area are influenced by the inflow of nutrient-rich Pacific waters and resulting higher marine primary production compared to the Kara, Laptev and East Siberian Seas (Codispoti et al., 2013).

Comparison of $N_2O$ depth profiles and surface water saturation, together with incubation data points at $N_2O$ consumption in the water column as one driver of locally observed surface water undersaturation. First, we found surface water undersaturation and uptake of atmospheric $N_2O$ in 55 of 88 stations (Figure 3f). Sediment uptake was only observed in two of 14 stations and much lower than sea-air fluxes. Second, both surface and bottom waters were undersatured in $N_2O$ at all 12 stations where $N_2O$ concentration significantly increased with depth, and seven of these stations also showed a significant increase in $N_2O$ saturation. These stations include the two ice-free stations and one of three ice-covered stations where $N_2O$ saturation in surface waters was below 60%. For example, at station AMK-82 6958, $N_2O$ concentration and saturation significantly ($p < 0.05$) decreased from 12 nM and 70% in bottom waters to 8 nM and 51% at the surface. These observations point at a sedimentary source at these stations, but suggest also $N_2O$ consumption in the water column, overall leading to increasing undersaturation towards the surface. Third, we directly observed net consumption of $N_2O$ in the water-only controls of the sediment incubations at 10 of 14 stations (Table S4 in Supporting Information S1). These samples are not representative for the entire water column, but demonstrate that $N_2O$ consumption can occur in bottom waters. Nitrous oxide consumption has been in the past largely associated with denitrification under anoxic conditions, which is in conflict with the oxygenation of the entire water column in the study region. More recent studies have demonstrated $N_2O$ consumption also in oxygenated surface waters, as indicated by a decrease in $N_2O$ concentration in sea water samples during incubation (Rees et al., 2021), and by tracing $^{15}N$ from $N_2O$ into organic matter (Cornejo et al., 2015; Farías et al., 2013). In addition, active nosZ genes that code for the enzyme $N_2O$ reductase have been detected in oxygenated surface waters at a range of locations (Coates & Wyman, 2017; Raes et al., 2016; Rees et al., 2021; Sun et al., 2017; Wyman et al., 2013). These studies provide compelling support for biological $N_2O$ consumption in oxygenated waters. It remains unclear at this point if this $N_2O$ consumption actually happens under oxic conditions, or at anoxic microsites. Active nosZ genes have been found also in bacteria associated with cyanobacterial colonies in oxygenated surface waters, suggesting that denitrification and $N_2O$ consumption could occur under sub- or anoxic conditions within the colony (Coates & Wyman, 2017). Such microsites might also exist in sinking organic aggregates (Bianchi et al., 2018; Wolgast et al., 1998) and might provide conditions suitable for $N_2O$ reduction also in our system. Taken together, our data suggest water column $N_2O$ consumption as an important component of $N_2O$ dynamics in the study area. Considering the limited importance of sediments as $N_2O$ sources, it is possible that also $N_2O$ production is dominated by water column processes, by nitrification or denitrification, including classic denitrification at anoxic microsites as outlined above, or nitrifier denitrification that has also been demonstrated under oxic conditions (Wrage-Mönnig et al., 2018). Direct evidence for water column $N_2O$ production in this system is however missing.

### 4.3. River Impact on Nitrogen Availability and $N_2O$ Concentrations

We originally hypothesized that nitrogen delivered from land would increase nitrogen availability in the water column and promote $N_2O$ production in these areas. In line with our expectations, we found that nitrogen input by large rivers led to elevated nitrogen concentrations in the water column of the Siberian shelf seas near the river mouths. The recently published Circum-Arctic Sediment CArbon DatabasE (Martens et al., 2021a, 2021b) complements our water column observations and shows elevated nitrogen concentrations also in surface

sediments near the Yenisey estuary and the Lena river delta (Figure 3g). Taken together, river-derived nitrogen might promote nitrogen availability for primary production and a range of nitrogen cycle processes including nitrification and denitrification near the river mouths. In addition, rivers might also directly transport $N_2O$ to the coastal ocean.

In contrast to our hypothesis, we found no support for a substantial enhancement of $N_2O$ concentrations near river mouths. Although nitrogen availability has been suggested to exert a primary control on $N_2O$ production, the relationship between elevated nitrogen near rivers and $N_2O$ concentrations was weak. Significant correlations with concentrations of different dissolved inorganic nitrogen (DIN) forms were primarily observed in the Indigirka plume, but were very weak in the Lena and absent in the Ob/Yenisey plumes. These observations do not support our hypothesis of terrigenous nitrogen input promoting net $N_2O$ production near river mouths or of direct $N_2O$ delivery by rivers, but suggest that other parameters have a stronger influence on $N_2O$ dynamics in the region. One such parameter might be turbidity that was significantly correlated with $N_2O$ concentrations in the Ob/Yenisey and Indigirka plumes. A connection between high $N_2O$ concentration and high turbidity has been frequently observed in estuaries (Abril et al., 2000; Barnes & Upstill-Goddard, 2011). The production of $N_2O$ in turbid waters might be facilitated by high nitrification rates, driven by high concentrations of particulate organic nitrogen, by the accumulation of bacteria around particles (Barnes & Upstill-Goddard, 2011), or by light-limitation of primary production that reduces competition for nitrogen by phytoplankton. High $N_2O$ in turbid waters might also stem from denitrification at anoxic microsites of particles (Liu et al., 2013). Taken together, the spatial distribution of $N_2O$ suggests an influence of both nitrogen and turbidity delivered by rivers, and large differences in dominant drivers across the Siberian shelf seas.

We here propose that the variation in $N_2O$ concentrations across the Siberian Arctic Ocean shelves might be partly explained by interactions between nitrogen availability and turbidity. The three river plumes showed contrasting relationships between DIN, turbidity and $N_2O$ in the mixed layer. For the Indigirka plume, both DIN and turbidity increased with proximity to the river mouth. Together, increasing substrate availability for nitrification and denitrification and increasing turbidity could favor higher $N_2O$ concentrations closer to the river. The Lena and Ob/Yenisey plumes showed opposing cross-shelf trends of these three parameters in the mixed layer. For the Ob/Yenisey plume, we observed the highest turbidity at two stations 150–220 km from the Ob (Figure 3b). These stations also had the highest $N_2O$ concentrations (Figure 3d), and were clearly distinct from the high-nitrogen, low-salinity waters near the river mouth. The Lena plume also showed a turbidity maximum at greater distance from the high-nitrogen, low-salinity waters near the coast (Figure 3b). For the Lena plume, we did not observe a significant correlation of $N_2O$ concentration and turbidity; a possible positive effect of turbidity on $N_2O$ might however have been neutralized by a negative effect of decreasing nitrogen concentration with distance from shore.

In addition, temperature has been suggested as a key control on high-latitude $N_2O$ dynamics. Higher temperature has been shown to favor denitrification over anammox (Canion et al., 2014; Rysgaard et al., 2004; Tan et al., 2020), that is, the anaerobic oxidation of ammonium by nitrite to $N_2$ that competes with denitrification for substrate and is thought not to produce $N_2O$ directly (Okabe et al., 2011). Mixed layer temperature significantly increased towards the Indigirka mouth, possibly adding to the stimulating effect of DIN and turbidity on $N_2O$ production near the river. By contrast, temperature significantly decreased towards the Lena mouth, which could have contributed to dampening $N_2O$ production close to the coast. Interactions between nitrogen availability, turbidity, and possibly temperature might have contributed to the contrasting cross-shelf trends in $N_2O$ concentration across the Siberian shelf seas.

### 4.4. Implications of Climate Change on $N_2O$ Dynamics in the Siberian Arctic Ocean

Anthropogenic climate warming is rapidly changing the Arctic Ocean. Projections include an increase in water temperature, decline of sea ice, and increased input of freshwater and a range of organic and inorganic compounds, fueled by land permafrost thaw. Both nitrogen input and turbidity are expected to increase with higher river transport (Bobrovitskaya et al., 2003; Doxaran et al., 2015; Frey & McClelland, 2009; Gordeev, 2006; Krickov et al., 2018) and accelerating coastal erosion (Nielsen et al., 2022). The correlations observed in this study make it possible that increasing nitrogen availability and turbidity will stimulate $N_2O$ production and $N_2O$ emissions on the Siberian Arctic Ocean shelves. The moderate $R^2$ of even the strongest correlations and the high variability

across river plumes however indicate confounding effects of multiple processes on $N_2O$ dynamics in this Arctic shelf system.

Rising temperatures might further directly stimulate a range of nitrogen cycle processes (Greaver et al., 2016), independent of changes in nitrogen loading or turbidity. Both $N_2O$ production by nitrification and denitrification, as well as $N_2O$ reduction in water column or sediments might increase, and the net effect on $N_2O$ will depend on the balance between production and consumption processes. Denitrification-derived $N_2O$ production is particularly sensitive to temperature, as denitrification outcompetes anammox at higher temperatures. Strongest warming effects are expected at northern high latitudes, where a doubling of sedimentary $N_2O$ production by denitrification has been projected until 2100 in the Representative Concentration Pathway (RCP) 8.5 scenario (Tan et al., 2020). Nitrous oxide production from sediments, but possibly also from water column denitrification might become more important on the Siberian Arctic Ocean shelves in the future.

Rising temperatures could also affect $N_2O$ fluxes by altering $N_2O$ solubility in the ocean water. Recent Earth System Models project an increase in Arctic Ocean sea surface temperature by 5°C (SSP 5–8.5 scenario; Kwiatkowski et al., 2020) and a decrease in salinity in the top 100 m by 1.5‰ until the end of the century (RCP 8.5 scenario; Koenigk et al., 2013). Even larger decreases are possible on a regional scale. For instance, a decrease by ca. 13%, that is, 3‰ salinity has been suggested for the near-coastal Laptev Sea (Fu et al., 2020) which already has a low salinity due to freshwater discharge by the Lena river. Increasing temperature strongly reduces the solubility of gases in the water, while freshening partly counteracts this effect. To illustrate the magnitude of the solubility effect, we tested how projected changes in temperature and salinity alone would influence $N_2O$ saturation and fluxes in the study area, without considering expected changes in wind speed, $N_2O$ production and consumption. A change in temperature by +5°C and in salinity by −1.5‰ would alter average $N_2O$ saturation from 94 ± 24% as observed here to 113 ± 29%. Fluxes of $N_2O$ would change from an uptake of 0.5 ± 12 μmol $m^{-2}$ $d^{-1}$ to the release of 7 ± 15 μmol $m^{-2}$ $d^{-1}$. An increase in atmospheric $N_2O$ mixing ratio by 60 ppb as projected by 2100 in SSP5-8.5 (IPCC, 2021) would counteract the decrease in $N_2O$ solubility, overall resulting in 96 ± 25% saturation and +0.3 ± 14 μmol $m^{-2}$ $d^{-1}$ $N_2O$ flux. The apparent discrepancy between average undersaturation and average positive fluxes results from slightly higher wind speeds at oversaturated stations observed here, and the large uncertainty range spans from positive to negative fluxes. Wind speed and $N_2O$ concentrations were kept at the observed values for this illustration. Given also the limited temporal coverage of our data, we emphasize that our calculations do not represent a realistic projection of future $N_2O$ emissions from the Siberian Arctic Ocean shelves, but demonstrate the sensitivity of $N_2O$ fluxes to warming-induced changes in solubility. Reduced $N_2O$ solubility will add to changes in wind speed as well as $N_2O$ production and consumption that are likely to follow large-scale alterations of the biogeochemical and physical regime in the study region. Our findings suggest that $N_2O$ production and consumption are strongly influenced by interactions among such biogeochemical and physical parameters, and point at water column processes as central players.

## Data Availability Statement

All data are available in Supporting Information S1 and in the Bolin Centre Database under the link https://bolin.su.se/data/wild-2023-nitrous-oxide-1 and the doi https://doi.org/10.17043/wild-2023-nitrous-oxide-1.

**Acknowledgments**

We thank the crew and scientific team of the SWERUS-C3 2014 and ISSS-2020 expeditions, and in particular the ISSS-2020 sediment team for sample collection. We further thank Joanna Sawicka for water sampling on SWERUS-C3 2014, and Tommaso Tesi for organic carbon and nitrogen analysis of ISSS-2020 sediments. This study was funded by the Swedish Research Council VR (Grant 2018-05489 to B.W., 621-2013-5297 and 2017-01601 to Ö.G.), the Swedish Research Council for Sustainable Development Formas (Grant 2018-01547 to B.W.), the European Research Council (ERC-AdG CC-TOP, Grant 695331 to Ö.G.), the Knut and Alice Wallenberg Foundation (KAW Grant 2011.0027 to Ö.G.), the Norwegian Research Council ("Bio-essential and toxic elements transformation and transport in the Arctic under pressure of Siberian Continental Shelf permafrost thawing" BEST-Siberian to E.Y.), the Russian Scientific Foundation (Grant 21-77-30001 to I.S. and O.D.), the Russian Ministry of Science and Higher Education (Grant "Priority-2030" to Tomsk State University; Grant 0128-2021-0001 to A.O. and E.Y.). The charter of the R/V *Akademik Mstislav Keldysh* was funded by Grant 021-2021-0010 from the Ministry of Science and Higher Education of the Russian Federation.

## References

Abril, G., Riou, S. A., Etcheber, H., Frankignoulle, M., De Wit, R., & Middelburg, J. J. (2000). Transient, tidal time-scale, nitrogen transformations in an estuarine turbidity maximum - Fluid mud system (the Gironde, South-West France). *Estuarine, Coastal and Shelf Science*, *50*(5), 703–715. https://doi.org/10.1006/ecss.1999.0598

Arévalo-Martínez, D. L., Steinhoff, T., Brandt, P., Körtzinger, A., Lamont, T., Rehder, G., & Bange, H. W. (2019). $N_2O$ emissions from the northern Benguela upwelling system. *Geophysical Research Letters*, *46*(6), 3317–3326. https://doi.org/10.1029/2018GL081648

Babbin, A. R., Keil, R. G., Devol, A. H., & Ward, B. B. (2014). Organic matter stoichiometry, flux, and oxygen control nitrogen loss in the ocean. *Science*, *344*(6182), 406–408. https://doi.org/10.1126/science.1248364

Bange, H. W., Kock, A., Pelz, N., Schmidt, M., Schütte, F., Walter, S., et al. (2019). Nitrous oxide in the northern Gulf of Aqaba and the central Red Sea. *Deep-Sea Research Part II: Topical Studies in Oceanography*, *166*(October 2018), 90–103. https://doi.org/10.1016/j.dsr2.2019.06.015

Barnes, J., & Upstill-Goddard, R. C. (2011). $N_2O$ seasonal distributions and air-sea exchange in UK estuaries: Implications for the tropospheric $N_2O$ source from European coastal waters. *Journal of Geophysical Research*, *116*(1), G01006. https://doi.org/10.1029/2009JG001156

Barnes, J., & Upstill-Goddard, R. C. (2018). The denitrification paradox: The role of $O_2$ in sediment $N_2O$ production. *Estuarine, Coastal and Shelf Science*, *200*(3), 270–276. https://doi.org/10.1016/j.ecss.2017.11.018

Bianchi, D., Weber, T. S., Kiko, R., & Deutsch, C. (2018). Global niche of marine anaerobic metabolisms expanded by particle microenvironments. *Nature Geoscience*, *11*(April), 1–6. https://doi.org/10.1038/s41561-018-0081-0

Bobrovitskaya, N. N., Kokorev, A. V., & Lemeshko, N. A. (2003). Regional patterns in recent trends in sediment yields of Eurasian and Siberian rivers. *Global and Planetary Change*, *39*(1–2), 127–146. https://doi.org/10.1016/S0921-8181(03)00021-3

Breider, F., Yoshikawa, C., Abe, H., Toyoda, S., & Yoshida, N. (2015). Origin and fluxes of nitrous oxide along a latitudinal transect in western North Pacific: Controls and regional significance. *Global Biogeochemical Cycles*, *29*(F), 1014–1027. https://doi.org/10.1002/2014GB004977

Brin, L. D., Giblin, A. E., & Rich, J. J. (2014). Environmental controls of anammox and denitrification in southern New England estuarine and shelf sediments. *Limnology and Oceanography*, *59*(3), 851–860. https://doi.org/10.4319/lo.2014.59.3.0851

Canion, A., Overholt, W. A., Kostka, J. E., Huettel, M., Lavik, G., & Kuypers, M. M. M. (2014). Temperature response of denitrification and anaerobic ammonium oxidation rates and microbial community structure in Arctic fjord sediments. *Environmental Microbiology*, *16*(10), 3331–3344. https://doi.org/10.1111/1462-2920.12593

Charpentier, J., Farías, L., & Pizarro, O. (2010). Nitrous oxide fluxes in the central and eastern South Pacific. *Global Biogeochemical Cycles*, *24*(3), 1–14. https://doi.org/10.1029/2008GB003388

Coates, C. J., & Wyman, M. (2017). A denitrifying community associated with a major, marine nitrogen fixer. *Environmental Microbiology*, *19*(12), 4978–4992. https://doi.org/10.1111/1462-2920.14007

Codispoti, L. A., Kelly, V., Thessen, A., Matrai, P., Suttles, S., Hill, V., et al. (2013). Synthesis of primary production in the Arctic Ocean: III. Nitrate and phosphate based estimates of net community production. *Progress in Oceanography*, *110*(December 2012), 126–150. https://doi.org/10.1016/j.pocean.2012.11.006

Cornejo, M., Murillo, A. A., & Farías, L. (2015). An unaccounted for $N_2O$ sink in the surface water of the eastern subtropical South Pacific: Physical versus biological mechanisms. *Progress in Oceanography*, *137*, 12–23. https://doi.org/10.1016/j.pocean.2014.12.016

Doxaran, D., Devred, E., & Babin, M. (2015). A 50% increase in the mass of terrestrial particles delivered by the Mackenzie River into the Beaufort Sea (Canadian Arctic Ocean) over the last 10 years. *Biogeosciences*, *12*(11), 3551–3565. https://doi.org/10.5194/bg-12-3551-2015

Dutton, G., Elkins, J. I., Hall, B., & ESRL, N. (2017). *Earth system research laboratory halocarbons and other atmospheric trace gases chromatograph for atmospheric trace species (CATS) measurements, Version 1*. NOAA National Centers for Environmental Information. https://doi.org/10.7289/V5X0659V

Elkins, J. W. (1980). Determination of dissolved nitrous oxide in aquatic systems by gas chromatography using electron-capture detection and multiple phase equilibration. *Analytical Chemistry*, *52*(2), 263–267. https://doi.org/10.1021/ac50052a011

Farías, L., Faúndez, J., Fernández, C., Cornejo, M., Sanhueza, S., & Carrasco, C. (2013). Biological $N_2O$ fixation in the Eastern South Pacific Ocean and marine cyanobacterial cultures. *PLoS One*, *8*(5), e63956. https://doi.org/10.1371/journal.pone.0063956

Farquharson, L. M., Mann, D. H., Swanson, D. K., Jones, B. M., Buzard, R. M., & Jordan, J. W. (2018). Temporal and spatial variability in coastline response to declining sea-ice in northwest Alaska. *Marine Geology*, *404*(July), 71–83. https://doi.org/10.1016/j.margeo.2018.07.007

Fenwick, L., Capelle, D., Damm, E., Zimmermann, S., Williams, W. J., Svein, V., & Tortell, P. D. (2017). Methane and nitrous oxide distributions across the North American Arctic Ocean during summer, 2015. *Journal of Geophysical Research: Oceans*, *122*(1), 390–412. https://doi.org/10.1002/2016JC012493.Received

Forster, G., Upstill-Goddard, R. C., Gist, N., Robinson, C., Uher, G., & Woodward, E. M. S. (2009). Nitrous oxide and methane in the Atlantic Ocean between 50°N and 52°S: Latitudinal distribution and sea-to-air flux. *Deep-Sea Research Part II: Topical Studies in Oceanography*, *56*(15), 964–976. https://doi.org/10.1016/j.dsr2.2008.12.002

Foster, S. Q., & Fulweiler, R. W. (2016). Sediment nitrous oxide fluxes are dominated by uptake in a temperate estuary. *Frontiers in Marine Science*, *3*(MAR), 1–13. https://doi.org/10.3389/fmars.2016.00040

Frame, C., Deal, E., Nevison, C. D., & Casciotti, K. L. (2014). $N_2O$ production in the eastern South Atlantic: Analysis of $N_2O$ stable isotopic and concentration data. *Global Biogeochemical Cycles*, *28*(11), 1262–1278. https://doi.org/10.1002/2013GB004790.Received

Frey, K. E., & McClelland, J. W. (2009). Impacts of permafrost degradation on arctic river biogeochemistry. *Hydrological Processes*, *23*(1), 169–182. https://doi.org/10.1002/hyp.7196

Fu, W., Moore, J. K., Primeau, F. W., Lindsay, K., & Randerson, J. T. (2020). A growing freshwater lens in the Arctic Ocean with sustained climate warming disrupts marine ecosystem function. *Journal of Geophysical Research: Biogeosciences*, *125*(12), 1–14. https://doi.org/10.1029/2020JG005693

Gordeev, V. V. (2006). Fluvial sediment flux to the Arctic Ocean. *Geomorphology*, *80*(1–2), 94–104. https://doi.org/10.1016/j.geomorph.2005.09.008

Greaver, T. L., Clark, C. M., Compton, J. E., Vallano, D., Talhelm, A. F., Weaver, C. P., et al. (2016). Key ecological responses to nitrogen are altered by climate change. *Nature Climate Change*, *6*(9), 836–843. https://doi.org/10.1038/nclimate3088

Günther, F., Overduin, P. P., Sandakov, A. V., Grosse, G., & Grigoriev, M. N. (2013). Short- and long-term thermo-erosion of ice-rich permafrost coasts in the Laptev Sea region. *Biogeosciences*, *10*(6), 4297–4318. https://doi.org/10.5194/bg-10-4297-2013

Heo, J.-M., Kim, S.-S., Kang, S.-H., Yang, E. J., Park, K.-T., Jung, J., et al. (2021). $N_2O$ dynamics in the western Arctic Ocean during the summer of 2017. *Scientific Reports*, *11*(1), 1–12. https://doi.org/10.1038/s41598-021-92009-1

Hersbach, H., Bell, B., Berrisford, P., Biavati, G., Horányi, A., Muñoz Sabater, J., et al. (2018). *ERA5 hourly data on single levels from 1979 to present*. Copernicus Climate Change Service (C3S) Climate Data Store (CDS). https://doi.org/10.24381/cds.adbb2d47

Hirota, A., Ijiri, A., Komatsu, D. D., Ohkubo, S. B., Nakagawa, F., & Tsunogai, U. (2009). Enrichment of nitrous oxide in the water columns in the area of the Bering and Chukchi Seas. *Marine Chemistry*, *116*(1–4), 47–53. https://doi.org/10.1016/j.marchem.2009.09.001

Holmes, R. M., McClelland, J. W., Peterson, B. J., Tank, S. E., Bulygina, E., Eglinton, T. I., et al. (2012). Seasonal and annual fluxes of nutrients and organic matter from large rivers to the Arctic Ocean and surrounding seas. *Estuaries and Coasts*, *35*(2), 369–382. https://doi.org/10.1007/s12237-011-9386-6

Hopkinson, C. S., Giblin, A. E., & Tucker, J. (2001). Benthic metabolism and nutrient regeneration on the continental shelf of Eastern Massachusetts, USA. *Marine Ecology Progress Series*, *224*(July 2015), 1–19. https://doi.org/10.3354/meps224001

Hopkinson, C. S., Giblin, A. E., Tucker, J., & Garritt, R. H. (1999). Benthic metabolism and nutrient cycling along an estuarine salinity gradient. *Estuaries*, *22*(4), 863–881. https://doi.org/10.2307/1353067

Humborg, C., Geibel, M. C., Anderson, L. G., Björk, G., Mörth, C. M., Sundbom, M., et al. (2017). Sea-air exchange patterns along the central and outer East Siberian Arctic Shelf as inferred from continuous $CO_2$, stable isotope, and bulk chemistry measurements. *Global Biogeochemical Cycles*, *31*(7), 1173–1191. https://doi.org/10.1002/2017GB005656

IPCC. (2021). Annex III: Tables of historical and projected well-mixed greenhouse gas mixing ratios and effective radiative forcing of all climate forcers. [F. J. Dentener, B. Hall, C. Smith (Eds.)]. In V. Masson-Delmotte, P. Zhai, A. Pirani, S. L. Connors, C. Péan, et al. (Eds.), *Climate 19 change 2021: The physical science basis. Contribution of Working Group I to the sixth assessment report 20 of the Intergovernmental Panel on Climate Change*. Cambridge University Press.

Jakobsson, M. (2002). Hypsometry and volume of the Arctic Ocean and its constituent seas. *Geochemistry, Geophysics, Geosystems*, *3*(5), 1–18. https://doi.org/10.1029/2001gc000302

Jakobsson, M., Mayer, L. A., Bringensparr, C., Castro, C. F., Mohammad, R., Johnson, P., et al. (2020). The international bathymetric chart of the Arctic Ocean version 4.0. *Scientific Data*, *7*(1), 1–14. https://doi.org/10.1038/s41597-020-0520-9

Jameson, B. D., Berg, P., Grundle, D. S., Stevens, C. J., & Juniper, S. K. (2021). Continental margin sediments underlying the NE Pacific oxygen minimum zone are a source of nitrous oxide to the water column. *Limnology and Oceanography Letters*, *6*(2), 68–76. https://doi.org/10.1002/lol2.10174

Johnson, M. T. (2010). A numerical scheme to calculate temperature and salinity dependent air-water transfer velocities for any gas. *Ocean Science*, *6*(4), 913–932. https://doi.org/10.5194/os-6-913-2010

Jones, B. M., Arp, C. D., Jorgenson, M. T., Hinkel, K. M., Schmutz, J. A., & Flint, P. L. (2009). Increase in the rate and uniformity of coastline erosion in Arctic Alaska. *Geophysical Research Letters*, *36*(3), 1–5. https://doi.org/10.1029/2008GL036205

Kitidis, V., Upstill-Goddard, R. C., & Anderson, L. G. (2010). Methane and nitrous oxide in surface water along the north-west Passage, Arctic Ocean. *Marine Chemistry*, *121*(1–4), 80–86. https://doi.org/10.1016/j.marchem.2010.03.006

Koenigk, T., Brodeau, L., Graversen, R. G., Karlsson, J., Svensson, G., Tjernström, M., et al. (2013). Arctic climate change in 21st century CMIP5 simulations with EC-Earth. *Climate Dynamics*, *40*(11–12), 2719–2743. https://doi.org/10.1007/s00382-012-1505-y

Krickov, I. V., Lim, A. G., Manasypov, R. M., Loiko, S. V., Shirokova, L. S., Kirpotin, S. N., et al. (2018). Riverine particulate C and N generated at the permafrost thaw front: Case study of western Siberian Rivers across a 1700 km latitudinal transect. *Biogeosciences*, *15*(22), 6867–6884. https://doi.org/10.5194/bg-15-6867-2018

Kwiatkowski, L., Torres, O., Bopp, L., Aumont, O., Chamberlain, M., Christian, J. R., et al. (2020). Twenty-first century ocean warming, acidification, deoxygenation, and upper-ocean nutrient and primary production decline from CMIP6 model projections. *Biogeosciences*, *17*(13), 3439–3470. https://doi.org/10.5194/bg-17-3439-2020

Lantuit, H., Overduin, P. P., Couture, N., Wetterich, S., Aré, F., Atkinson, D., et al. (2012). The Arctic Coastal Dynamics database: A new classification scheme and statistics on arctic permafrost coastlines. *Estuaries and Coasts*, *35*(2), 383–400. https://doi.org/10.1007/s12237-010-9362-6

Liu, T., Xia, X., Liu, S., Mou, X., & Qiu, Y. (2013). Acceleration of denitrification in turbid rivers due to denitrification occurring on suspended sediment in oxic waters. *Environmental Science and Technology*, *47*(9), 4053–4061. https://doi.org/10.1021/es304504m

Manning, C. C. M., Zheng, Z., Fenwick, L., McCulloch, R. D., Damm, E., Izett, R. W., et al. (2022). Interannual variability in methane and nitrous oxide concentrations and sea-air fluxes across the North American Arctic Ocean (2015–2019). *Global Biogeochemical Cycles*, *36*(4), 1–25. https://doi.org/10.1029/2021GB007185

Martens, J., Romankevich, E., Semiletov, I., Wild, B., van Dongen, B., Vonk, J., et al. (2021a). CASCADE – The Circum-Arctic Sediment CArbon DatabasE. *Earth System Science Data*, *13*(6), 2561–2572. https://doi.org/10.5194/essd-13-2561-2021

Martens, J., Romankevich, E., Semiletov, I., Wild, B., van Dongen, B., Vonk, J., et al. (2021b). *The Circum-Arctic Sediment Carbon Database — CASCADE*. Bolin Centre Database. https://doi.org/10.17043/cascade-2

Mazur, C. I., Al-Haj, A. N., Ray, N. E., Sanchez-Viruet, I., & Fulweiler, R. W. (2021). Low denitrification rates and variable benthic nutrient fluxes characterize Long Island Sound sediments. *Biogeochemistry*, *154*(1), 37–62. https://doi.org/10.1007/s10533-021-00795-7

McClelland, J. W., Holmes, R. M., Peterson, B. J., Raymond, P. A., Striegl, R. G., Zhulidov, A. V., et al. (2016). Particulate organic carbon and nitrogen export from major Arctic rivers. *Global Biogeochemical Cycles*, *30*(5), 629–643. https://doi.org/10.1002/2015GB005351.Received

Naqvi, S. W. A., Jayakumar, D. A., Narvekar, P. V., Naik, H., Sarma, V. V. S. S., D'Souza, W., et al. (2000). Increase marine production of $N_2O$ due to intensifying anoxia on the Indian continental shelf. *Nature*, *408*(November), 346–349. https://doi.org/10.1038/35042551

Nielsen, D. M., Pieper, P., Barkhordarian, A., Overduin, P., Ilyina, T., Brovkin, V., et al. (2022). Increase in Arctic coastal erosion and its sensitivity to warming in the twenty-first century. *Nature Climate Change*, *12*(3), 263–270. https://doi.org/10.1038/s41558-022-01281-0

Novikova, A., Belova, N., Baranskaya, A., Aleksyutina, D., Maslakov, A., Zelenin, E., et al. (2018). Dynamics of permafrost coasts of Baydaratskaya Bay (Kara Sea) based on multi-temporal remote sensing data. *Remote Sensing*, *10*(9), 1481. https://doi.org/10.3390/rs10091481

Okabe, S., Oshiki, M., Takahashi, Y., & Satoh, H. (2011). $N_2O$ emission from a partial nitrification-anammox process and identification of a key biological process of $N_2O$ emission from anammox granules. *Water Research*, *45*(19), 6461–6470. https://doi.org/10.1016/j.watres.2011.09.040

Osadchiev, A. A., Pisareva, M. N., Spivak, E. A., Shchuka, S. A., & Semiletov, I. P. (2020). Freshwater transport between the Kara, Laptev, and East-Siberian seas. *Scientific Reports*, *10*(1), 13041. https://doi.org/10.1038/s41598-020-70096-w

Osadchiev, A. A., Silvestrova, K., & Myslenkov, S. (2020). Wind-driven coastal upwelling near large river deltas in the Laptev and east-Siberian seas. *Remote Sensing*, *12*(5), 1–25. https://doi.org/10.3390/rs12050844

Ouyang, Z., Qi, D., Zhong, W., Chen, L., Gao, Z., Lin, H., et al. (2021). Summertime evolution of net community production and $CO_2$ flux in the Western Arctic Ocean. *Global Biogeochemical Cycles*, *35*(3), 1–24. https://doi.org/10.1029/2020GB006651

Paulmier, A., Ruiz-Pino, D., & Garcon, V. (2008). The oxygen minimum zone (OMZ) off Chile as intense source of $CO_2$ and $N_2O$. *Continental Shelf Research*, *28*(20), 2746–2756. https://doi.org/10.1016/j.csr.2008.09.012

Peralta-Ferriz, C., & Woodgate, R. A. (2017). The dominant role of the East Siberian Sea in driving the oceanic flow through the Bering strait—Conclusions from GRACE ocean mass satellite data and in situ mooring observations between 2002 and 2016. *Geophysical Research Letters*, *44*(22), 11472–11481. https://doi.org/10.1002/2017GL075179

Prairie, Y. T. (1996). Evaluating the predictive power of regression models. *Canadian Journal of Fisheries and Aquatic Sciences*, *53*(3), 490–492. https://doi.org/10.1139/cjfas-53-3-490

Raes, E. J., Bodrossy, L., Van De Kamp, J., Holmes, B., Hardman-Mountford, N., Thompson, P. A., et al. (2016). Reduction of the powerful greenhouse gas $N_2O$ in the south-eastern Indian ocean. *PLoS One*, *11*(1), 1–11. https://doi.org/10.1371/journal.pone.0145996

Randall, K., Scarratt, M., Levasseur, M., Michaud, S., Xie, H., & Gosselin, M. (2012). First measurements of nitrous oxide in Arctic sea ice. *Journal of Geophysical Research*, *117*(5), 2–9. https://doi.org/10.1029/2011JC007340

Ravishankara, A. R., Daniel, J. S., & Portmann, R. W. (2009). Nitrous oxide ($N_2O$): The dominant ozone-depleting substance emitted in the 21st century. *Science*, *326*(5949), 123–125. https://doi.org/10.1126/science.1176985

Ray, N. E., Hancock, B., Brush, M. J., Colden, A., Cornwell, J., Labrie, M. S., et al. (2021). A review of how we assess denitrification in oyster habitats and proposed guidelines for future studies. *Limnology and Oceanography: Methods*, *19*(10), 714–731. https://doi.org/10.1002/lom3.10456

R Core Team. (2018). *R: A language and environment for statistical computing*. R Foundation for Statistical Computing. Retrieved from https://www.r-project.org/

Rees, A. P., Brown, I. J., Jayakumar, A., Lessin, G., Somerfield, P. J., & Ward, B. B. (2021). Biological nitrous oxide consumption in oxygenated waters of the high latitude Atlantic Ocean. *Communications Earth & Environment*, *2*(1), 1–8. https://doi.org/10.1038/s43247-021-00104-y

Rowe, G. T., Clifford, C. H., Smith, K. L. J., & Hamilton, P. L. (1975). Benthic nutrient regeneration and its coupling to primary productivity in coastal waters. *Nature*, *255*(5505), 215–217. https://doi.org/10.1038/255215a0

Rysgaard, S., Glud, R. N., Risgaard-Petersend, N., & Dalsgaard, T. (2004). Denitrification and anammox activity in Artic marine sediments. *Limnology and Oceanography*, *49*(5), 1493–1502. https://doi.org/10.4319/lo.2004.49.5.1493

Sanders, T., Fiencke, C., Fuchs, M., Haugk, C., Juhls, B., Mollenhauer, G., et al. (2022). Seasonal nitrogen fluxes of the Lena River Delta. *Ambio*, *51*(2), 423–438. https://doi.org/10.1007/s13280-021-01665-0

Saucier, W. (2003). *Principles of meteorological analysis*. Dover Publications.

Seitzinger, S. P., Nixon, S. W., & Pilson, M. E. Q. (1984). Denitrification and nitrous oxide production in a coastal marine ecosystem. *Limnology and Oceanography*, *29*(1), 73–83. https://doi.org/10.4319/lo.1984.29.1.0073

Semiletov, I., Dudarev, O., Luchin, V., Charkin, A., Shin, K. H., & Tanaka, N. (2005). The East Siberian Sea as a transition zone between Pacific-derived waters and Arctic shelf waters. *Geophysical Research Letters*, *32*(10), 1–5. https://doi.org/10.1029/2005GL022490

Shakhova, N., Semiletov, I., Salyuk, A., Yusupov, V., Kosmach, D., & Gustafsson, Ö. (2010). Extensive methane venting to the atmosphere from sediments of the East Siberian Arctic Shelf. *Science*, *327*(5970), 1246–1251. https://doi.org/10.1126/science.1182221

Shaw, W. J., Stanton, T. P., McPhee, M. G., Morison, J. H., & Martinson, D. G. (2009). Role of the upper ocean in the energy budget of Arctic sea ice during SHEBA. *Journal of Geophysical Research*, *114*(6), 1–21. https://doi.org/10.1029/2008JC004991

Sturm, K., Grinham, A., Werner, U., & Yuan, Z. (2016). Sources and sinks of methane and nitrous oxide in the subtropical Brisbane River estuary, South East Queensland, Australia. *Estuarine, Coastal and Shelf Science*, *168*, 10–21. https://doi.org/10.1016/j.ecss.2015.11.002

Sun, X., Humborg, C., Mörth, C. M., & Brüchert, V. (2021). The importance of benthic nutrient fluxes in supporting primary production in the Laptev and East Siberian shelf seas. *Global Biogeochemical Cycles*, *35*(7), e2020GB006849. https://doi.org/10.1029/2020GB006849

Sun, X., Jayakumar, A., & Ward, B. B. (2017). Community composition of nitrous oxide consuming bacteria in the oxygen minimum zone of the Eastern Tropical South Pacific. *Frontiers in Microbiology*, *8*(JUN), 1–11. https://doi.org/10.3389/fmicb.2017.01183

Tan, E., Zou, W., Zheng, Z., Yan, X., Du, M., Hsu, T. C., et al. (2020). Warming stimulates sediment denitrification at the expense of anaerobic ammonium oxidation. *Nature Climate Change*, *10*(4), 349–355. https://doi.org/10.1038/s41558-020-0723-2

Terhaar, J., Lauerwald, R., Regnier, P., Gruber, N., & Bopp, L. (2021). Around one third of current Arctic Ocean primary production sustained by rivers and coastal erosion. *Nature Communications*, *12*(1), 1–10. https://doi.org/10.1038/s41467-020-20470-z

Thibodeau, B., Bauch, D., & Voss, M. (2017). Nitrogen dynamic in Eurasian coastal Arctic ecosystem: Insight from nitrogen isotope. *Global Biogeochemical Cycles*, *31*(5), 836–849. https://doi.org/10.1002/2016GB005593

Thornton, B. F., Geibel, M. C., Crill, P. M., Humborg, C., & Mörth, C. M. (2016). Methane fluxes from the sea to the atmosphere across the Siberian shelf seas. *Geophysical Research Letters*, *43*(11), 5869–5877. https://doi.org/10.1002/2016GL068977

Tian, H., Xu, R., Canadell, J. G., Thompson, R. L., Winiwarter, W., Suntharalingam, P., et al. (2020). A comprehensive quantification of global nitrous oxide sources and sinks. *Nature*, *586*(7828), 248–256. https://doi.org/10.1038/s41586-020-2780-0

Toyoda, S., Kakimoto, T., Kudo, K., Yoshida, N., Sasano, D., Kosugi, N., et al. (2021). Distribution and production mechanisms of $N_2O$ in the Western Arctic Ocean. *Global Biogeochemical Cycles*, *35*(4), 1–15. https://doi.org/10.1029/2020GB006881

Valderrama, J. C. (1981). The simultaneous analysis of total nitrogen and total phosphorus in natural waters. *Marine Chemistry*, *10*(2), 109–122. https://doi.org/10.1016/0304-4203(81)90027-X

Voss, M., Bange, H. W., Dippner, J. W., Middelburg, J. J., Montoya, J. P., & Ward, B. (2013). The marine nitrogen cycle: Recent discoveries, uncertainties and the potential relevance of climate change. *Philosophical Transactions of the Royal Society B: Biological Sciences*, *368*(1621), 20130121. https://doi.org/10.1098/rstb.2013.0121

Wanninkhof, R. (2014). Relationship between wind speed and gas exchange over the ocean revisited. *Limnology and Oceanography: Methods*, *12*(JUN), 351–362. https://doi.org/10.4319/lom.2014.12.351

Wanninkhof, R., Asher, W. E., Ho, D. T., Sweeney, C., & McGillis, W. R. (2009). Advances in quantifying air-sea gas exchange and environmental forcing. *Annual Review of Marine Science*, *1*, 213–244. https://doi.org/10.1146/annurev.marine.010908.163742

Weiss, R. F., & Price, B. A. (1980). Nitrous oxide solubility in water and seawater. *Marine Chemistry*, *8*(4), 347–359. https://doi.org/10.1016/0304-4203(80)90024-9

Wolgast, D. M., Carlucci, A. F., & Bauer, J. E. (1998). Nitrate respiration associated with detrital aggregates in aerobic bottom waters of the abyssal NE Pacific. *Deep Sea Research Part II: Topical Studies in Oceanography*, *45*(4–5), 881–892. https://doi.org/10.1016/s0967-0645(98)00006-x

Wrage-Mönnig, N., Horn, M. A., Well, R., Müller, C., Velthof, G., & Oenema, O. (2018). The role of nitrifier denitrification in the production of nitrous oxide revisited. *Soil Biology & Biochemistry*, *123*(April), A3–A16. https://doi.org/10.1016/j.soilbio.2018.03.020

Wu, M., Chen, L., Zhan, L., Zhang, J., Li, Y., & Liu, J. (2017). Spatial variability and factors influencing the air-sea $N_2O$ flux in the Bering Sea, Chukchi Sea and Chukchi Abyssal Plain. *Atmosphere*, *8*(65), 1–13. https://doi.org/10.3390/atmos8040065

Wyman, M., Hodgson, S., & Bird, C. (2013). Denitrifying alphaproteobacteria from the Arabian Sea that express nosZ, the gene encoding nitrous oxide reductase, in oxic and suboxic waters. *Applied and Environmental Microbiology*, *79*(8), 2670–2681. https://doi.org/10.1128/AEM.03705-12

Yang, S., Chang, B. X., Warner, M. J., Weber, T. S., Bourbonnais, A. M., Santoro, A. E., et al. (2020). Global reconstruction reduces the uncertainty of oceanic nitrous oxide emissions and reveals a vigorous seasonal cycle. *Proceedings of the National Academy of Sciences of the United States of America*, *117*(22), 11954–11960. https://doi.org/10.1073/pnas.1921914117

Zhan, L., Zhang, J., Ouyang, Z., Lei, R., Xu, S., Qi, D., et al. (2021). High-resolution distribution pattern of surface water nitrous oxide along a cruise track from the Okhotsk Sea to the western Arctic Ocean. *Limnology and Oceanography*, *66*(S1), S401–S410. https://doi.org/10.1002/lno.11604

Zhang, J., Liyang, Z., Chen, L., Li, Y., & Chen, J. (2015). Coexistence of nitrous oxide undersaturation and oversaturation in the surface and subsurface of the western Arctic Ocean. *Journal of Geophysical Research: Oceans*, *120*(12), 8392–8401. https://doi.org/10.1002/2015JC011245.Received